6-2014

Investigation of the Mechanism of Binding of Perfluoroalkyl Acids with Human Serum Albumin Using an Improved Approach to Equilibrium Dialysis

Michael Morris
Union College - Schenectady, NY

Investigation of the Mechanism of Binding of Perfluoroalkyl Acids with Human Serum Albumin Using an Improved Approach to Equilibrium Dialysis

By

Michael Anthony Morris

****

Submitted in partial fulfillment
of the requirements for
Honors in the Department of Chemistry

UNION COLLEGE

June, 2014

ABSTRACT

MORRIS, MICHAEL A Investigation of the mechanism of binding of perfluoroalkyl acids with human serum albumin using an improved approach to equilibrium dialysis. Department of Chemistry, June 2014.

ADVISOR: Laura A. MacManus-Spencer

Perfluoroalkyl acids (PFAAs) are used to produce many consumer products, but their bioaccumulative and toxic properties and their global persistence in the environment are major concerns. In particular, PFAAs have been shown to accumulate in the blood, liver, and kidneys of organisms. As such, it is important to elucidate the toxicokinetics of PFAAs by quantitatively and qualitatively characterizing the binding mechanism of PFAAs to human serum albumin (HSA). In this study, the binding of PFAAs to HSA are studied via a high-throughput equilibrium dialysis method that utilizes the 96-well Equilibrium Dialyzer coupled with sample quantitation using liquid chromatography tandem-mass spectrometry (LC-MS/MS). This equilibrium dialysis method provides an efficient and direct way to measure protein-ligand binding constants. Using the described methods, it was determined that HSA has approximately two binding sites associated with a high affinity (10^5 M^{-1}) as well as approximately fifteen binding sites associated with a lower affinity (10^3 M^{-1}) for perfluorooctanoic acid (PFOA). These binding constants indicate that PFOA binds to HSA with the same affinity as some endogenous ligands, which illuminates the toxicity concerns of these chemicals. Future applications of this method could include measuring the binding constants of other PFAAs to HSA, characterizing the binding mechanism of PFAAs to HSA by examining the effect of various pH and ionic strength values with respect to binding strength, and measuring binding constants of PFAAs to myoglobin and hemoglobin.

Acknowledgements

This project would not be possible without the help and support from several people. I am indebted to Professor Laura MacManus-Spencer for providing the opportunity to do research in her lab; for her continuous help, dedication, and patience throughout the progress of this project; and for being a wonderful educator, mentor, and chemist at Union College. Words cannot express how grateful I am for all of the help Professor MacManus-Spencer has given me during my time at Union College. I would like to thank previous LAMS lab thesis students, Paul Hebert and Megan O'Connor, for their prior work and research on this project. I also would like to thank my fellow lab mate, Taera Kim, for being a great friend and for her incessant support throughout senior year while we were doing research in the LAMS lab, applying to graduate school, and surviving quantum chemistry.

Lastly, I would like to thank the following resources for financially supporting this project:

- Professor MacManus-Spencer
- The Lee Davenport '37 Summer Research Fellowship
- The Union College Student Research Grant Program
- The Union College Presidential Green Grant Program

Table of Contents

List of Figures

List of Tables

1. Introduction

i. Relevance of perfluoroalkyl acids

Perfluoroalkyl acids (PFAAs) are perfluorinated chemicals that are used to produce various industrial and consumer products, such as non-stick cookware; liquid repellants for paper, packaging, textile, leather, and carpet goods; and industrial surfactants, additives and coatings.[1] The unique physical and chemical properties of PFAAs, such as their stability and resistance to water and oil, make them attractive for industrial and commercial use.[1,2] However, due to the stability of PFAAs, they are effectively non-degradable by most physical and metabolic processes, which allows these chemicals to persist and accumulate in the environment and in organisms.[1-3] Although PFAAs are valuable for industrial and commercial applications, they pose serious environmental and biological threats. In fact, in recent decades, these chemicals have been confirmed as persistent, bioaccumulative, and toxic contaminants, and their global distribution in the environment is worrisome.[1-3]

Due to increased environmental and toxicological concerns about PFAAs in recent years, U.S. industries that use PFAAs for industrial purposes, such as Dupont and the 3M Company, have phased out the use of long-chain PFAAs (seven or more fluorinated carbons) and have replaced them with shorter-chain PFAAs (up to six or fewer fluorinated carbons).[4] Despite this effort, long-chain PFAAs that have been introduced to the environment will endure globally for decades. In addition, the continued use of PFAAs industrially, despite having shorter fluorocarbon chains, still poses environmental and health concerns. As such, it is imperative to study the fate of PFAAs

in the environment and in organisms in order to elucidate their environmental behavior and biological hazards.

ii. Chemistry of PFAAs

PFAAs are synthetic compounds that are derived from alkyl carboxylates and sulfonates in which their hydrogen atoms are substituted with fluorine and have carbon chain lengths between 1-14 carbons.[1,2] The skeletal formulae of typical perfluorocarboxylates (PFCAs) and perfluorosulfonates (PFSAs) of varying chain length are displayed in Figure 1. Due to the strength of the carbon-fluorine bond (≥461 kJ/mol),[5] the presence of three lone pairs of electrons surrounding each fluorine atom, and the effective shielding of the carbon backbone by the fluorine atoms,[1] PFAAs are able to resist degradation by strong acids and bases, oxidizing agents, reductants, photolytic processes, physical processes, and metabolic processes, which allows these chemicals to endure in the environment and in organisms for an extended period of time.[1,2] Moreover, the extensive fluorination of PFAAs gives rise to their unique and industrially attractive physical and chemical properties, such as their high chemical stability, non-flammability, low surface tension, hydrophobicity, and lipophobicity.[1,2] In addition, the high electronegativity of the fluorine atoms makes PFAAs strongly acidic molecules. In fact, PFAAs have estimated pK_a values ranging from -0.2 to 0[6] and consequently exist almost exclusively as anions under environmental and physiological conditions.[1,7] As expected from their stability and resistance to degradation, PFAAs have long elimination half-lives in humans; for instance, perfluorooctanoic acid (PFOA) has an estimated elimination half-life of 3.8 years in human females.[8] Interestingly enough, the elimination half-lives of various PFAAs differ among species and between genders.[2] For instance, the

elimination half-life of perfluorooctanesulfonic acid (PFOS) ranges from 100 days in adult rats to 5.4 years in humans.[9] Furthermore, the elimination half-life of PFOA in adult female rats is 2-4 hours, but in adult male rats, it is 4-6 days.[10]

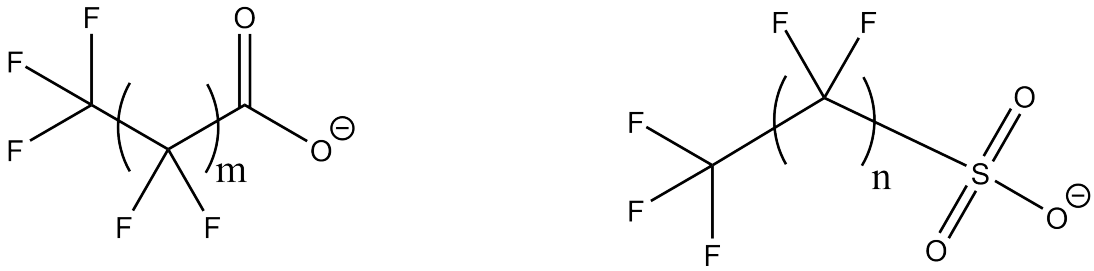

m = 1, 2, 3, 4, 5, 6, 7, 8, 9, 10 n = 3, 5, 7

Figure 1. The general structures of perfluorocarboxylates (PFCAs, left) and perfluorosulfonates (PFSAs, right) with the chain lengths indicated. Structures are shown in the deprotonated form since PFAAs exist as anions under most biological and environmental conditions.[1,7]

It is important to mention, from a biochemical standpoint, that PFAAs are structurally similar to some endogenous ligands that bind to vital proteins in organisms. For example, short-chain fatty acids are structurally analogous to PFCAs in that both contain a hydrophilic carboxylate head group and a hydrophobic tail. The structural similarities among PFCAs and short-chain fatty acids are demonstrated in Figure 2. Because of this structural resemblance, PFAAs have the potential to compete with short-chain fatty acids for binding to specific proteins and enzymes. If a PFAA successfully binds to a protein, it could potentially inhibit the protein's intended functions; thus, PFAAs have the potential to adversely affect organisms, and the long elimination half-lives of PFAAs in humans magnify this toxicity concern. However, despite their structural similarity, PFAAs behave chemically different than fatty acids in some ways. For example, PFAAs are lipophobic,[1,2] due to their rigid fluorocarbon tails and the low surface energy brought by the strongly-polarized carbon-fluorine bond,[11] whereas fatty acids are lipophilic.

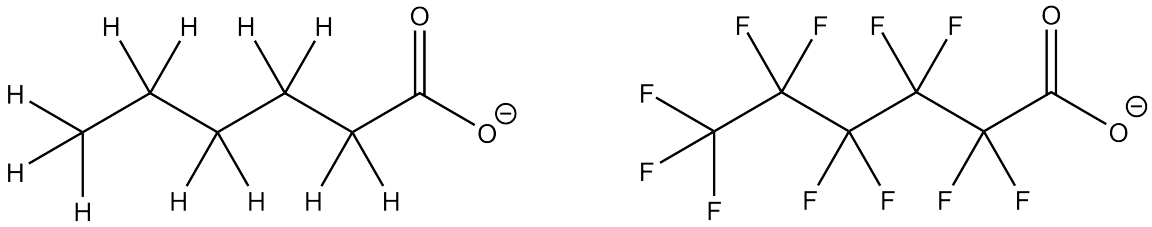

Figure 2. Structural comparisons of hexanoic acid (common name, caproic acid), a short-chain fatty acid, left, and perfluorohexanoic acid (PFHxA), right. The two compounds are shown in their anionic forms for comparison.

iii. Bioaccumulation patterns and toxicokinetics of PFAAs

Because of their unique physical properties, PFAAs exhibit unusual bioaccumulation patterns and toxicokinetics compared to typical hydrophobic organic contaminants. For example, PFAAs do not accumulate in adipose tissue, where hydrophobic contaminants tend to accrue, but rather in body compartments that are abundant in highly-charged chemical species, such as proteins. Consequently, PFAAs often aggregate in the blood,[12-16] liver, and kidneys[2,3,17-22] of organisms. The bioaccumulation of PFAAs in these areas is concerning since these biological components have vital functions in vertebrate animals, whereas bioaccumulation in adipose tissue is less important toxicologically since its main function is to provide energy storage and insulation.

The toxicokinetics of PFAAs in mammals have been well studied, and three key features of their distribution and protein interactions have been characterized. First, PFAAs accumulate in the blood plasma[12-16] and exhibit high binding affinities to serum albumin.[23-28] Second, PFAA transport into cells is postulated to be mediated by passive diffusion and by active transport via organic anion transporter (OAT) proteins.[29,30] Some OAT proteins, like the human OAT4 and URAT-1 proteins, are renal transport proteins that control the reabsorption of organic anions from the urine to the blood, and are hypothesized to be responsible for the extended elimination half-lives of several PFAAs.[30] Third, PFAAs exhibit binding interactions with fatty acid binding proteins (FABPs), which are expressed in many different cell types, and consequently act as relevant PFAA sinks in tissues.[31-33] Among these protein interactions, PFAA binding to serum albumin is considered to be more toxicologically pertinent because serum albumin

is the most abundant protein in mammalian blood[34] and since the blood frequently contains the highest concentrations of PFAAs. As such, serum albumin, including its human, bovine, and rat homologs, is often used to study PFAA-protein interactions. In addition, serum albumin can reversibly bind to a variety of ligands, making it an excellent model to study both the physiological fate of PFAAs and the ability of PFAAs to compete with endogenous ligands.

iv. Human serum albumin

Since the 19th century, human serum albumin (HSA) has been established as the most abundant protein in the circulatory system, typically found at a concentration of approximately 5 g per 100 mL; it is found in every tissue in the body.[34] This protein is produced in the liver and has a half-life of 19 days in circulation in the human body.[34] HSA has a molecular weight of 66,245 Da and consists of a single polypeptide composed of 585 amino acid residues.[35] The monomeric protein contains three homologous domains (I, II, and III), each with its own sub-domains, and these domains are most likely derived from gene multiplication.[36] The three-dimensional crystal structure of HSA has been solved at a 2.5 Å resolution and is displayed in Figure 3.[37]

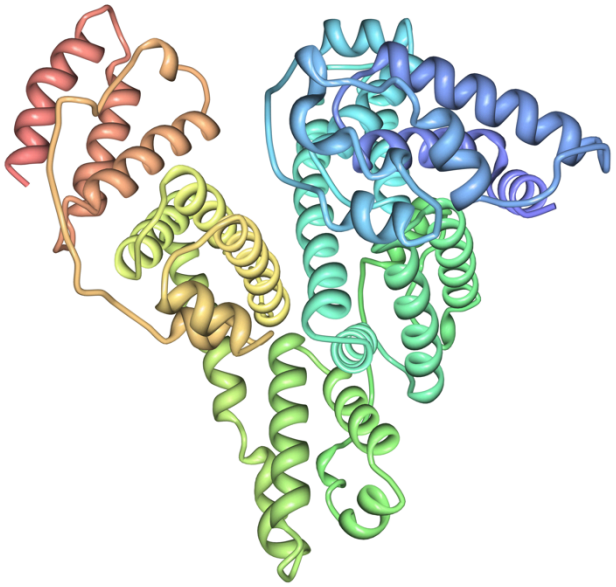

Figure 3. The three-dimensional crystal structure of HSA solved at 2.5 Å. The monomeric protein has three domains and contains a variety of binding sites for ligands.[36] This image was obtained from Protein Data Bank using the Protein Workshop software (PDB ID 1AO6).[37]

In addition, HSA has a variety of critical functions in the circulatory system, including maintaining blood pH and pressure, transporting fatty acids, removing oxygen free radicals, and reversibly binding to a variety of endogenous and exogenous ligands.[35] Such endogenous and exogenous ligands include transition metals like Cu^{2+} and Zn^{2+}, short-chain fatty acids, amino acids, proteins, metabolites, and drugs.[35, 38-40] The ability of HSA to reversibly bind to numerous ligands makes it an excellent model to examine the binding of PFAAs to serum proteins, both to understand the physiological fate of PFAAs and to investigate the potential of PFAAs to compete with endogenous ligands.

v. Prior studies of PFAA-serum albumin binding

Previous studies of PFAA-serum albumin binding have employed direct methods, such as equilibrium dialysis, and indirect methods, such as spectroscopic techniques, and established that PFAAs bind with relatively high affinity to serum albumin (see Table 1). For example, Bischel *et al*. extensively studied the binding interactions between PFAAs and bovine serum albumin (BSA, the homolog to HSA in cows) using a traditional equilibrium dialysis method and determined that the binding constants are on the order of 10^6 M^{-1}, varying with fluorocarbon chain length and ionic head group.[24, 27] In addition, Hebert and MacManus-Spencer developed a fluorescence model to probe the binding of medium- to long-chain PFAAs to HSA and estimated that the binding affinities are on the order of 10^4 M^{-1}.[25] Agreeing with the data obtained from Hebert *et al*., O'Connor and MacManus-Spencer have used fluorescence and also estimated HSA-PFAA binding constants to be on the order of 10^4 M^{-1}, varying with fluorocarbon chain length and ionic head group.[28]

Additional published studies, which employed various experimental techniques to measure serum albumin-PFOA binding affinities, also reported similar binding constants, reported in Table 1. These binding affinities range from 10^3 to 10^6 M^{-1}, which highlights some method disagreement among the experimental techniques utilized in these studies.

Table 1. Serum albumin-PFOA binding affinities (quantified as the association constant, K_a) from published studies that utilized different experimental techniques.

Protein-ligand system	K_a (M^{-1})	Experimental Technique	Source
HSA-PFOA	10^5	Fluorescence spectroscopy	Chen *et al*. (2009)[23]
HSA-PFOA	10^4	Equilibrium dialysis	Wu *et al*. (2009)[41]
HSA-PFOA	10^3	^{19}F NMR and micro-desalting separation	Han *et al*. (2003)[42]
HSA-PFOA	10^5	Potentiometric methods	Messina *et al*. (2005)[43]
BSA-PFOA	10^6	Equilibrium dialysis	Bischel *et al*. (2010)[24] and (2011)[27]
BSA-PFOA	10^5	Fluorescence spectroscopy	MacManus-Spencer *et al*. (2010)[26]
HSA-PFOA	10^4	Fluorescence spectroscopy	Hebert *et al*. (2010)[25]
HSA-PFOA	10^4	Fluorescence spectroscopy and ^{19}F NMR	O'Connor *et al.* (unpublished work)[28]

vi. Protein-ligand binding kinetics and quantitation

The binding interactions between a protein and a ligand, such as a drug or a molecule of interest, can be characterized by measuring the binding affinity between the two molecules using chemical kinetics. Biochemists quantify protein-ligand affinity by measuring the dissociation constant, K_d, for a particular protein-ligand system. The dissociation constant, K_d, is defined as the ratio of the products of the concentrations of the dissociated species to the concentration of the complex at equilibrium.[44] Specifically, in the case of protein-ligand binding, the dissociation constant is defined as the products of the concentrations of free protein and ligand divided by the concentration of the protein-ligand complex (Equation 4).[44]

A protein binds to its corresponding ligand according to the laws of mass action, which assumes reversible binding:[44]

$$\text{Protein} + \text{Ligand} \underset{k_{\text{off}}}{\overset{k_{\text{on}}}{\rightleftharpoons}} \text{Protein} \cdots \text{Ligand}$$

The association rate constant, k_{on}, is a second-order rate constant, and thus has units of $M^{-1}s^{-1}$, because the association rate it expresses depends both on the concentration of free ligand and the concentration of available binding sites in the protein.[45,46] The association rate constant (k_{on}) is proportional to the forward rate of the reaction:

$$\text{Rate} = [\text{Protein}]\,[\text{Ligand}]\,k_{\text{on}} \quad \textbf{(1)}$$

The dissociation rate constant, k_{off}, is a first-order rate constant, and thus has units of s^{-1}, because the dissociation rate depends only on the concentration of protein binding sites occupied with bound ligand.[45,46] The dissociation rate constant (k_{off}) is proportional to the reverse rate of the reaction:

$$\text{Rate} = [\text{Protein} \cdots \text{Ligand}]\,k_{\text{off}} \quad \textbf{(2)}$$

The reaction reaches equilibrium when the forward and reverse reaction rates are equal; that is, when the rate at which protein-ligand complexes are formed is equal to the rate at which protein-ligand complexes dissociate into their constituent components. Therefore, at equilibrium, Equations 1 and 2 are equal:

$$[\text{Protein}]\,[\text{Ligand}]\,k_{\text{on}} = [\text{Protein} \cdots \text{Ligand}]\,k_{\text{off}} \quad \textbf{(3)}$$

If Equation 3 is rearranged such that the ratio of the dissociation rate constant and the association rate constant is isolated on one side of the equation, we obtain the dissociation constant, K_d:

$$\frac{[\text{Protein}]\,[\text{Ligand}]}{[\text{Protein}\cdots\text{Ligand}]} = \frac{k_{\text{off}}}{k_{\text{on}}} = K_{\text{d}} \qquad \textbf{(4)}$$

Thus, the dissociation constant, K_d, can also be defined as the ratio of the dissociation rate constant (k_{off}) to the association rate constant (k_{on}) for a protein-ligand system at equilibrium. From Equation 4, the units of K_d can be derived as M, which makes this quantity mathematically convenient for further calculations. In addition, the dissociation constant is inversely proportional to protein-ligand binding affinity, so a smaller K_d value signifies stronger protein-ligand binding. The K_d is the inverse of the association constant (K_a), which has units of M^{-1} and is colloquially referred to as the binding constant for a protein-ligand system (Equation 5). Lastly, the association constant is proportional to protein-ligand binding affinity; thus, a larger K_a value indicates stronger protein-ligand binding.

$$\frac{[\text{Protein}\cdots\text{Ligand}]}{[\text{Protein}]\,[\text{Ligand}]} = \frac{k_{\text{on}}}{k_{\text{off}}} = K_{\text{a}} \qquad \textbf{(5)}$$

vii. Equilibrium dialysis

As mentioned, there are many techniques that can be used to measure the binding affinity between a protein and a ligand (*i.e.*, the K_a value of the protein-ligand system), including spectroscopic approaches as well as more direct methods, such as equilibrium dialysis. Equilibrium dialysis is the preferred method because it can be used to directly and accurately measure the relationship between ligand binding (K_a) and bound ligand concentration for protein-ligand systems, a benefit that spectroscopic methods cannot exploit.[47] Moreover, since protein-ligand binding is examined at kinetic equilibrium in

equilibrium dialysis, the method reduces the possibility of non-specific binding and therefore provides more accurate measurements of K_a values.[47]

In equilibrium dialysis, a dialysis membrane with a specific molecular weight cut off (MWCO) separates two chambers: one containing protein and the other containing ligand (in this case, PFAAs). The dialysis membrane prevents the protein molecules from diffusing across to the other chamber containing ligand, while the ligand can freely diffuse across the membrane and bind to the protein. Once equilibrium has been reached, the concentration of free ligand is measured, from which the bound concentration is calculated.[48] A schematic summary of the equilibrium dialysis method is shown in Figure 4.

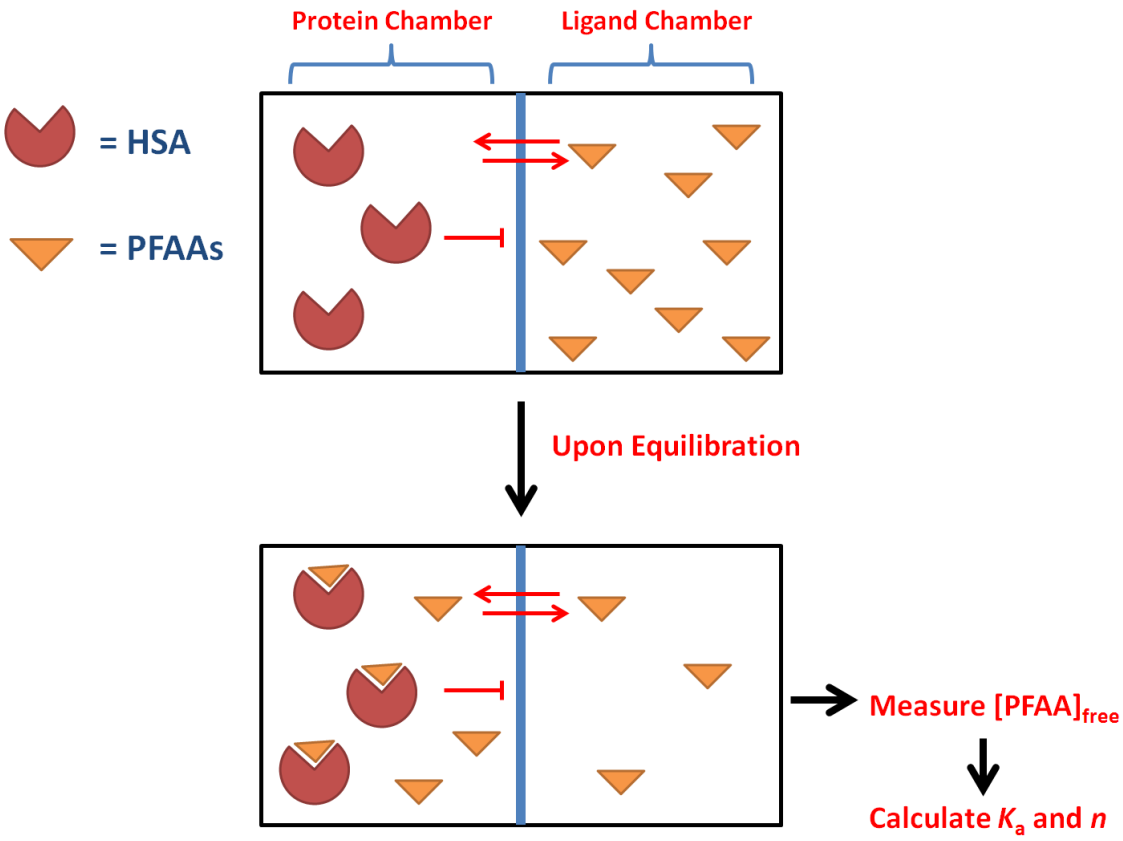

Figure 4. A schematic diagram of an equilibrium dialysis method to measure protein-ligand binding affinities. Adapted from Harvard Appartus.[49]

Upon studying several ligand:protein mole ratios, the relationship between binding and ligand concentration can be determined, which can then be used to calculate the number of binding sites (n) and the ligand affinity (K_a) through the construction and curve-fitting of a binding isotherm plot.[48] A sample binding isotherm plot is shown in Figure 5. In a binding isotherm, the binding coefficient ($\bar{v}$) or fractional saturation, defined as the ratio of bound ligand concentration to protein concentration, is plotted as a function of free ligand concentration; the shape of the plot typically resembles a hyperbolic curve. Lastly, it is important to note that when half of the available binding

sites in a protein are occupied, the binding coefficient is equal to 0.5 (the half-maximal saturation), and the free ligand concentration is equivalent to K_d.

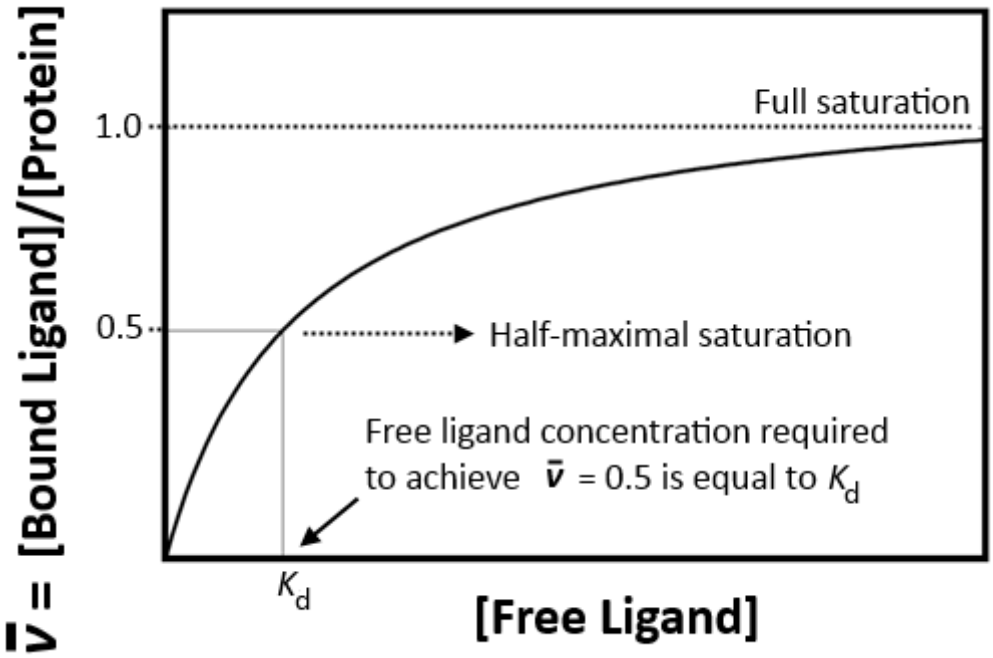

Figure 5. A binding isotherm plots the binding coefficient ($\bar{v}$) as a function of free ligand concentration, which typically generates a hyperbolic curve. This image was adapted from Kuriyan *et al*.[50]

Although equilibrium dialysis provides an accurate and direct way to measure binding constants, the traditional method has been shown to be cumbersome and slow. The traditional method of equilibrium dialysis consists of inserting a dialysis bag containing the protein and ligand of interest into a beaker filled with buffered solution, waiting for equilibration, and measuring unbound ligand concentration. However, this method is slow and cumbersome because only one mole ratio and one solution condition can be tested at one time, it requires large sample volumes, and the experimental setup is

time-consuming. Fortunately, these shortcomings of equilibrium dialysis have been addressed through the introduction of 96-well dialysis plates, which are commercially available through a variety of companies. For example, the 96-well equilibrium dialyzer (Harvard Apparatus) contains 96 individual wells, each with its own MWCO dialysis membrane. This allows one to conduct up to 96 individual binding experiments at one time, in which the PFAA:protein mole ratios and the solution conditions can be varied. Furthermore, the 96-well equilibrium dialyzer uses small volumes (up to 300 μL) of protein and ligand solutions; thus, it is less wasteful when it comes to solution preparation compared to the traditional methods of equilibrium dialysis.

In these equilibrium dialysis assays, the concentrations of free and bound ligand can be determined using liquid chromatography-tandem mass spectrometry (LC-MS/MS), a highly sensitive and selective method for the quantitation of organic chemicals, such as PFAAs.

viii. Liquid chromatography-tandem mass spectrometry (LC-MS/MS)

Liquid chromatography-tandem mass spectrometry (LC-MS/MS) is a powerful analytical instrument that couples high performance liquid chromatography (HPLC) and mass spectrometry to analyze small organic molecules and biomolecules. In LC-MS/MS, the HPLC is used to physically separate a mixture of chemical species due to their differential interactions with the stationary phase, and the mass spectrometer provides further chemical separation via mass-to-charge (*m/z*) selectivity as well as quantitation by measuring the ion abundance for each chemical species.[51]

In HPLC, high pressure is applied to force solvent (the mobile phase) through a packed column, containing a layer of densely-packed, microporous silica beads, which

act as a support for the stationary phase (e.g., an octadecyl carbon chain, C_{18}, in the case of reverse phase chromatography). The mixture of analytes is then mixed with the mobile phase and loaded onto the column via an autosampler. In the column, the analytes are separated due to their differential interactions with the stationary phase, which results in each analyte eluting from the column at a different time; thus, each analyte has a unique retention time in the column. Therefore, HPLC yields a separation of a mixture of chemical species due to their differences in retention time in the column. A detector, such as a UV/Vis spectrophotometer, is used to visualize the separation and quantify separated analytes. Computer software is used to generate a chromatogram, which is a plot of detector response (*e.g.*, absorbance signal) as a function of time.[51]

The most commonly used type of HPLC is reverse phase liquid chromatography, in which the stationary phase is nonpolar and the mobile phase is more polar. In reverse phase HPLC, a mixture of compounds is separated based on differences in analyte polarity and their differential interactions with the stationary and mobile phases. In this scheme, a polar compound will preferentially interact with the mobile phase and thus spends less time interacting with the nonpolar stationary phase, which results in a fast elution from the column and a short retention time. However, a nonpolar compound will exhibit thermodynamically-favorable interactions with the nonpolar stationary phase and thus spend more time in the column, which results in a slower elution from the column and a longer retention time.[51]

In addition to UV/Vis absorption detectors, other types of detectors may be coupled to an HPLC. In LC-MS/MS, a triple quadrupole mass analyzer with an electron multiplier serves as the detector. After a mixture of compounds is separated by reverse-

phase HPLC, they are transferred to the coupled triple quadrupole mass spectrometer for mass analysis via an ion source, such as electrospray ionization (ESI). ESI is a soft ionization technique that serves as the "connector" between liquid chromatography and mass spectrometry in LC-MS. In ESI, a voltage is applied to the liquid sample after it leaves the column, and the combination of a strong electric field at the nebulizer outlet and the coaxial flow of N_2 gas creates an aerosol of gaseous ions. It is important to note that the gas phase ions consist of the same ions found in the original liquid sample. Once the analyte's ions enter the mass spectrometer, its ions are filtered through a series of mass analyzers based on their *m/z* values. A common mode of mass analysis in a triple quadrupole mass spectrometer is multiple reaction monitoring (MRM). In MRM analysis, the precursor ion is selected in the first mass analyzer (first quadrupole). The quadrupole mass analyzer selects the ion of interest, the precursor ion, by filtering ions according to their *m/z* values. Specifically, a quadrupole consists of four poles, such that the adjacent poles have a voltage of opposite polarity applied to them. In order to filter an ion of interest, a coupled AC and DC voltage ramp is applied to the four poles, which affects the trajectories of ions as they travel through the center of the quadrupole. At a particular AC/DC voltage ratio, only ions with a specific *m/z* have a successful trajectory through the quadrupole and into the next chamber, whereas all other ions collide with the poles and are therefore lost before they enter the collision chamber. In the collision chamber (a hexapole), an inert gas fragments the precursor ion via a process called collision-induced dissociation. Next, the fragment ions enter the second mass analyzer (another quadrupole), which separates the fragment ions based on their *m/z* values; the ions are then detected by an electron multiplier detector. Computer software is used to generate a

mass spectrum, which is a plot of signal intensity as a function of *m/z*, for an analyte's precursor and fragment ions.[51,52] The various steps of MRM are summarized in Figure 6.

MRM analysis is useful for analytical studies for it provides high sensitivity and selectivity through the reduction of chemical noise and the correlation of specific fragment ions with their respective precursor ions. In addition, the selection and collision processes are fast, which allows for the analysis of multiple analytes in a single run. In fact, the analytes do not necessarily need to be chromatographically separated for MRM analysis to work since mass analyzers can select ions based on their *m/z* values. The mass analysis provided by MRM makes it possible to selectively and sensitively measure the concentration of unbound PFAAs from equilibrium dialysis assays.

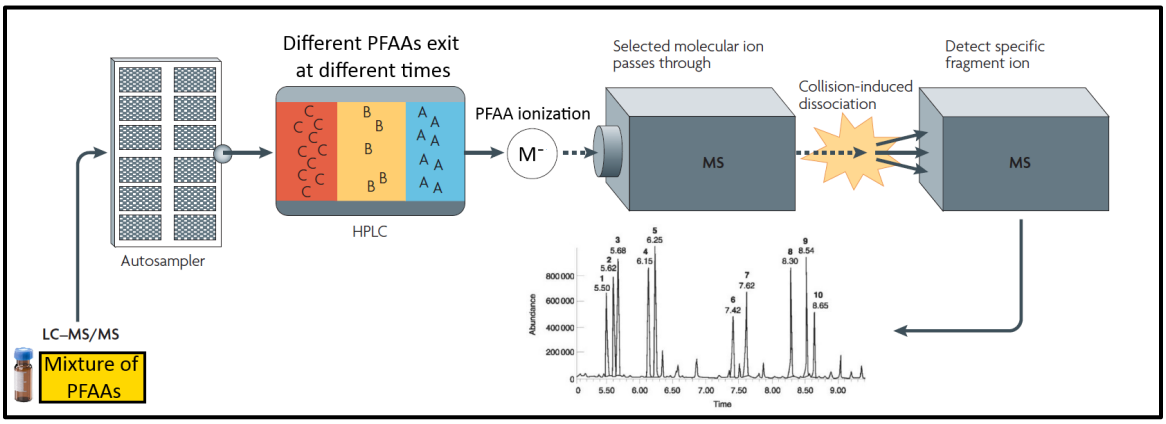

Figure 6. A schematic diagram that summarizes the steps involved in MRM in an LC-MS/MS. Image adapted from Last *et al*.[53]

ix. Experimental goals

Interactions between PFAAs and serum proteins have been studied previously using equilibrium dialysis and spectroscopic approaches; however, many of these studies are deficient in experimental parameters that allow a greater understanding of the

bioaccumulation patterns, toxicokinetics, and binding mechanisms between PFAAs and serum proteins. For example, some studies only focused on one or two PFAAs,[41-43] and those that did examine PFAAs with varying chain lengths did not take into account solution conditions (i.e., pH and ionic strength),[24-26] except for two previous studies[27,54] and O'Connor and MacManus-Spencer.[28] Furthermore, some spectroscopic methods, such as fluorescence, cannot be used to study the binding interactions between short-chain PFAAs and HSA, since short-chain PFAAs fail to cause a conformational change in HSA.[25,28] The improved equilibrium dialysis method, described and implemented in this study, can solve these issues since (1) this method is high-throughput and can accommodate the probing of various experimental parameters, such as varying PFAA chain length as well as solution conditions, and (2) our method allows one to measure directly the relationship between ligand binding (K_a) and ligand concentration.

The main goal of this study is to implement a more efficient and improved approach to the use of equilibrium dialysis to study PFAA-protein binding. Using our improved equilibrium dialysis method, we obtained PFAA-HSA binding affinities that can be compared to: (1) PFAA-BSA binding affinities determined by a traditional method of equilibrium dialysis in studies by Bischel *et al*.[27] (2010) and (2) PFAA-HSA binding affinities determined through fluorescence studies executed by O'Connor and MacManus-Spencer[28] as well as the other prior studies.[25] By obtaining binding affinities that agree with those obtained using the traditional equilibrium dialysis method, we can establish our improved equilibrium dialysis method as a valid method to characterize PFAA-protein binding. We also seek to compare our results to those obtained using

fluorescence spectroscopy in order to investigate the apparent discrepancy in binding affinities.

II. Materials and Methods

A. Materials

96-well Equilibrium Dialyzer plates and a plate rotator were obtained from Harvard Apparatus (Holliston, MA). Human serum albumin (HSA; ≥ 99%, essentially fatty acid and γ-globulin free) was obtained from Sigma-Aldrich (St. Louis, MO), and 66,245 Da was used as the molecular weight.[35] Pentafluoropropionic acid (PFPrA; 97%), perfluorobutanesulfonic acid potassium salt (PFBS-K^+; 98%), perfluoropentanoic acid (PFPnA; 97%), perfluorohexanoic acid (PFHxA; 97%), perfluorohexanesulfonic acid potassium salt (PFHxS-K^+; 98%), perfluoroheptanoic acid (PFHpA; 99%), perfluorooctanoic acid (PFOA; 96%), perfluorooctanesulfonic acid potassium salt (PFOS-K^+; 98%), perfluorononanoic acid (PFNA; 97%), perfluoroundecanoic acid (PFUnA; 95%), and perfluorododecanoic acid (PFDoA; 95%) were also obtained from Sigma-Aldrich. Perfluorobutanoic acid (PFBA; 99%), perfluorooctanoic acid (PFOA; 96%), and perfluorodecanoic acid (PFDA; 96%) were obtained from Acros Organics (Morris Plains, NJ) through Fisher Scientific USA (Pittsburgh, PA). Sodium phosphate monobasic (99.3%, monohydrate), sodium phosphate dibasic (99.3%, anhydrous), ammonium hydroxide (certified ACS Plus), methanol (Optima LC-MS grade, 0.1-micron filtered), water (Optima LC-MS grade, 0.03-micron filtered), ammonium acetate, and polypropylene microcentrifuge tubes (2 mL) were obtained from Fisher Scientific. Polypropylene centrifuge tubes (15- and 50-mL) were obtained from Corning

Incorporated (Corning, NY). HPLC autosampler vials and caps were obtained from Kinesis, Inc. (Malta, NY). A C_{18} Gemini column (50 x 2.0 mm x 5 μm) was obtained from Phenomenex, Inc. (Torrance, CA). A C_{18} Targa Sprite column (40 x 2.1 mm x 5 μm) was obtained from Higgins Analytical (Mountain View, CA). A C_{18} Eclipse column (4.6 x 150 x 5 μm) was obtained from Agilent Technologies (Santa Clara, CA). A mass-labeled ($^{13}C_4$) PFOA internal standard (50 μg/mL) was obtained from Wellington Laboratories, Inc. (Ontario, Canada).

B. Methods

i. Sample preparation

Sodium phosphate buffers (50 mM total phosphate concentration; at pH 7) were prepared from sodium phosphate monobasic and sodium phosphate dibasic in LC-MS grade water. Stock solutions of PFAAs were prepared either in pure LC-MS grade methanol, a 70:30 mixture of LC-MS grade methanol and 0.01% ammonium hydroxide, or 50 mM sodium phosphate buffer (at pH 7) in 10- or 50-mL polypropylene centrifuge tubes, as needed. If the PFAA was not soluble in the stock solution, the solution was sonicated in a water bath at about 40 °C until dissolved using the Bransonic Tabletop Ultrasonic Cleaner 3510 (Branson Ultrasonic Corporation; Danbury, CT). A purity-corrected stock solution of 500 μM HSA in 50 mM sodium phosphate buffer (at pH 7) was prepared in a 50-mL glass volumetric flask. This solution was prepared fresh for every experiment.

ii. Equilibrium dialysis

The 96-well Equilibrium Dialyzer is a two-sided dialysis plate, containing 12 columns by 8 rows of 96 individual wells. Using this dialysis plate, a column of eight

wells on the "ligand" side of the plate was sealed with caps (from Harvard Apparatus). The plate was inverted to the "protein" side of the plate, in which 200 µL of 500 µM HSA in 50 mM sodium phosphate buffer (at pH 7) were pipetted into the appropriate wells; after, these wells containing protein were sealed with caps. Then, the plate was inverted to the "ligand" side and the caps covering the appropriate wells were removed. Using a micropipette, 200 µL of PFAA (of known concentration) in 50 mM sodium phosphate buffer (at appropriate pH) was pipetted into the appropriate wells and then sealed with caps. The plate was then secured onto a plate rotator and rotated (using the fastest rotation speed) at room temperature until equilibrium was achieved. Upon equilibration, samples from both sides of the plate were collected and stored in either HPLC autosampler vials or in 2 mL microcentrifuge tubes at 4 °C until analysis by LC-MS/MS, when the concentration of unbound PFAAs was measured in the "ligand" side samples. Equilibrium dialysis experiments were performed either in singlicate, duplicate, or triplicate, depending on the experiment.

iii. LC-MS/MS quantitative analysis of PFAAs

Samples analyzed by LC-MS/MS were pipetted into HPLC autosampler vials and diluted with a combination of the following solutions: mass-labeled [$^{13}C_4$]-PFOA internal standard in LC-MS grade water (10 nM final concentration), 50 mM sodium phosphate buffer (at pH 7), and 70:30 mixture of LC-MS grade methanol and 0.01% ammonium hydroxide. The volumes of each solution were in a 1:2:2 proportion, respectively. For all LC-MS/MS experiments, a blank (which contained the mass-labeled internal standard in water, 70:30 mixture of LC-MS grade methanol and 0.01% ammonium hydroxide, and 50 mM sodium phosphate buffer at appropriate pH) and a double blank (which contained

LC-MS grade water, 70:30 mixture of LC-MS grade methanol and 0.01% ammonium hydroxide, and 50 mM sodium phosphate buffer (at pH 7) were included for analysis. An Agilent 1200 series HPLC and Agilent 6410B triple quadrupole mass spectrometer were used to analyze the samples. Separation of analytes was achieved by reverse-phase HPLC using three different columns and methods: Gemini C_{18} column (Phenomenex), Sprite C_{18} column (Higgins Analytical), and Eclipse C_{18} (Agilent Technologies). In method 1, the Gemini C_{18} column was utilized, and the mobile phase was a gradient mixture consisting of different percentages of 2 mM ammonium acetate in LC-MS grade water and pure LC-MS grade methanol over time. The gradient used to separate a mixture of PFAAs, including PFPrA, PFBA, PFBS, PFPnA, PFHxA, PFHxS, PFHpA, PFOA, PFOS, PFNA, PFDA, PFUnA, and PFDoA, using the Gemini C_{18} column is displayed in Table 2.

Table 2. The HPLC gradient used to separate a mixture of PFAAs studied using method 1.

Time (min)	Percentage of LC-MS grade methanol
0	30%
2	30%
3	70%
4	70%
5	50%
6	50%
7	70%
8	70%
9	90%

Later studies utilized two other methods since the Gemini C_{18} column is no longer functional. In method 2, the Targa Sprite C_{18} column was used with an isocratic mobile phase to separate a single PFAA per experiment; information pertaining to method 2 is displayed in Table 3. In method 3, the Eclipse C_{18} column was utilized and a similar isocratic method was used to elute a single PFAA per experiment; information pertaining to method 3 is also displayed in Table 3. Methods 2 and 3 later proved to be unsuccessful due to column pressure issues that remain unresolved.

Table 3. The isocratic mobile phases used to separate analytes for methods 2 and 3.

Method and column	Analyte eluted	Percentage of LC-MS grade methanol	Approximate analyte retention time (min)
Method 2; Sprite C_{18} (Higgins Analytical)	PFOA	55%	4.44
Method 3; Eclipse C_{18} (Agilent Technologies)	PFOA	65%	4.65

For methods 1 and 3, the following parameters were held constant throughout all separations. For all gradient and isocratic methods, a 40 µL injection volume, 1 mL/min flow rate, and 400 bar maximum pressure were used. Furthermore, the mass spectrometer was operated in negative electrospray ionization (ESI) mode with multiple reaction monitoring (MRM) analysis, with a 60 psi nebulizer pressure, 12 L/min gas flow, 350 °C gas temperature kept constant for all analyses. For method 2, the following parameters were utilized: 0.5 mL/min flow rate, 400 bar maximum pressure limit, negative ESI mode with MRM analysis, 40 psi nebulizer pressure, 10 L/min gas flow, and 350 °C gas temperature. The raw data obtained from the LC-MS/MS were processed using MassHunter Qualitative and Quantitative software (Agilent Technologies; Santa Clara,

CA) and were analyzed in Microsoft Office Excel (Microsoft Corporation; Redmond, WA) and KaleidaGraph graphical analysis software (Synergy Software Systems; Dubai, United Arab Emirates).

The three MRM methods were optimized by using the MassHunter Optimizer software (Agilent Technologies; Santa Clara, CA), which determined the relevant transition ions to be monitored for each analyte along with fragmentor voltages and collision energies. For all three methods, Table 4 summarizes the transition ions monitored, their corresponding fragmentor voltages and collision energies, and the quantifier and qualifier ions for all analytes studied.

Table 4. The MRM parameters used in this study.

Analyte	Transition type	MRM transition (*m/z*)	Fragmentor Voltage (V)	Collision Energy (V)
PFBA	Quantifier	213 → 169	50	0
PFOA	Quantifier	413 → 369	65	4
	Qualifier	413 → 169	65	16
PFDoA	Quantifier	613 → 569	80	4
	Qualifier	613 → 169	80	24
[$^{13}C_4$]-PFOA (ISTD)	Quantifier	417 → 372	60	4

A nested calibration curve was designed to contain standard solutions (of a particular PFAA or a mixture of PFAAs) within a linear concentration range of 0.150 – 6000 nM. Using a PFAA stock solution of known concentration, the nested calibration standards were prepared via nested serial dilutions. Each diluted standard was pipetted

into an HPLC autosampler vial and was further diluted using 10 nM mass-labeled internal standard, 50 mM sodium phosphate buffer (at appropriate pH), 70:30 mixture of LC-MS grade methanol and 0.01% ammonium hydroxide, and/or LC-MS grade water. The standards were "matrix-matched" to the samples (i.e., the standards had the same proportions, by volume and concentration, of solvents, buffers, and internal standards). The standard solutions were then analyzed via LC-MS/MS to measure the concentration of the PFAA standards. Using MassHunter Quantitative software (Agilent Technologies; Santa Clara, CA), a standard curve using the nested calibration standards was generated and the standards with 70% – 130% accuracy, with 1/x weighting, were only kept. For all PFAA-protein binding experiments, the PFAA standard solutions were made fresh and were analyzed, using the LC-MS/MS, in tandem with the protein binding experiment samples.

iv. Equilibration time determination

In order to establish the amount of time needed for a PFAA and HSA to reach equilibrium using equilibrium dialysis, multiple samples of 500 μM HSA and 10 μM of a specific PFAA were tested at different time points (between 18 – 120 hours) using the 96-well Equilibrium Dialyzer. At each time point, the appropriate sample was collected from the "ligand" side of the plate, and the concentration of free PFAA was measured using LC-MS/MS. A plot of percentage of PFAA bound versus time (in hours) was constructed. The desired equilibration time occurs when the percentage of PFAA bound to HSA approaches 100%, so the time at which this occurs is the optimal equilibration time for the PFAA and HSA. We determined that a 48-hour equilibration time for all

HSA-PFAA experiments was sufficient for binding analysis (shown in the Results and Discussion section).

v. HSA-PFOA binding experiments to measure protein-ligand affinity

In this experiment, seventeen PFOA:HSA mole ratios were tested using the 96-well Equilibrium Dialyzer in triplicate, in which the HSA concentration remained constant at 500 μM: 0.01:1, 0.02:1, 0.05:1, 0.1:1, 0.2:1, 0.4:1, 0.8:1, 1:1, 1.2:1, 1.4:1, 1.6:1, 2:1, 3:1, 3.6:1, 4:1, 8:1, and 16:1. After 48 hours of equilibration, the appropriate sample was collected from the "free-ligand" side of the plate and was subsequently diluted in a HPLC autosampler vial. The free PFOA concentration was measured using LC-MS/MS for each mole ratio sample in tandem with freshly prepared PFOA standards. The bound PFOA concentration was calculated by subtracting the measured free PFOA concentration value from the nominal initial concentration. The binding coefficient was calculated by dividing the bound PFOA concentration by the HSA concentration. Since this experiment was performed in triplicate, the average free PFOA concentrations and average binding coefficients, along with their standard deviations, were calculated. A binding isotherm plot was constructed by plotting the average binding coefficient as a function of average free PFOA concentration.

vi. Curve-fitting the binding isotherm plot via binding class models

Using KaleidaGraph software, the binding isotherm plot was curve-fitted using a nonlinear regression function that assumes a two independent binding site model. Since proteins often have more than one binding site for the same ligand, it is necessary to take the number of binding sites, *n*, into account when creating a model. Thus, if the binding

events are independent, then the binding coefficient ($\bar{\upsilon}$) for a protein that contains n binding sites can be expressed as:

$$\bar{\upsilon} = n\sum_{i=1}^{n} \upsilon_i \quad \textbf{(6)}$$

If there is only one binding site class site associated with one K_a value, then equation 6 becomes the one-binding class model:

$$\bar{\upsilon} = \frac{n_1 K_a [\mathrm{PFOA}]_{\mathrm{free}}}{1 + (K_a [\mathrm{PFOA}]_{\mathrm{free}})} \quad \textbf{(7)}$$

However, if there are two different classes of binding sites with unique binding affinities, then equation 6 becomes the two-binding class model:

$$\bar{\upsilon} = \frac{n_1 K_{a,1} [\mathrm{PFOA}]_{\mathrm{free}}}{1 + (K_{a,1} [\mathrm{PFOA}]_{\mathrm{free}})} + \frac{n_2 K_{a,2} [\mathrm{PFOA}]_{\mathrm{free}}}{1 + (K_{a,2} [\mathrm{PFOA}]_{\mathrm{free}})} \quad \textbf{(8)}$$

Equation 7 was used in KaleidaGraph to generate a best-fit curve function and determine the values for n_1, n_2, $K_{a,1}$, and $K_{a,2}$.

3. Results and Discussion

i. Development of a quantitative LC-MS/MS method for the analysis of PFAAs

Three different quantitative LC-MS/MS methods for the analysis of PFAAs were developed during the course of this project. Each method corresponds to a specific HPLC column; that is, method 1 utilizes the Phenomenex Gemini C_{18} column, method 2 utilizes the Higgins Sprite C_{18} column, and method 3 utilizes the Agilent Eclipse C_{18} column. Method 1 is no longer used since the Phenomenex Gemini C_{18} column is broken, which resulted in the development of method 2. However, the Higgins Sprite C_{18} column is currently experiencing unresolved pressure issues, so method 3 was developed as a

temporary placeholder for method 2. However, the Agilent Eclipse C_{18} column is currently experiencing pressure and leaking issues, so the development of a new quantitative LC-MS/MS method using a new column may be required for the continuation of this project.

Using method 1 (using the Gemini C_{18} column), the retention time for PFOA was 4.566 min, and a 6-μM standard yielded a peak area of 1.21×10^6 counts•min; the TIC MRM chromatogram for this standard is shown in Figure 7.

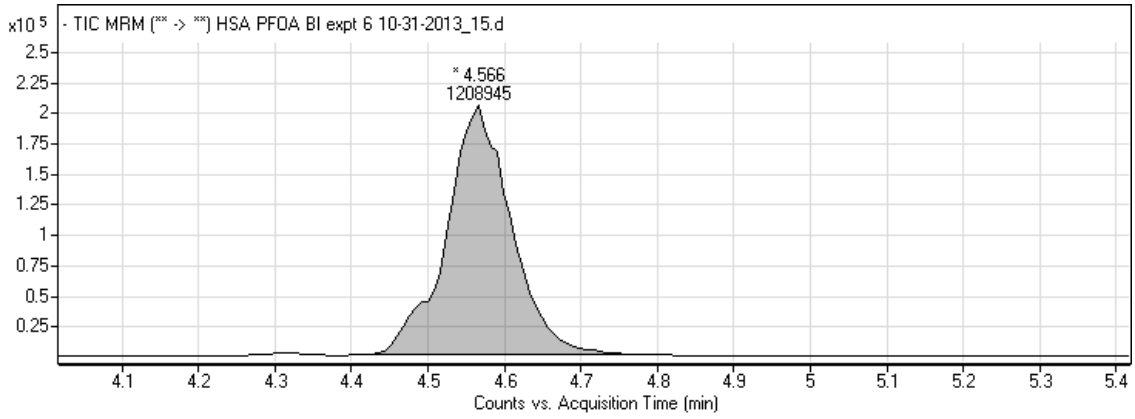

Figure 7. The TIC MRM chromatogram of 6 μM PFOA obtained using method 1. PFOA has a retention time of 4.566 min and a peak area of 1.21×10^6 counts•min.

Using Agilent's MassHunter Qualitative software, the MRM transition chromatograms were extracted from the 6-μM PFOA TIC chromatogram that was obtained using method 1. The MRM transitions include 413 → 369, 413 → 219, and 413 → 169 *m/z* for PFOA and 417 → 372 *m/z* for [$^{13}C_4$]-PFOA (internal standard); these MRM chromatograms are displayed in the Appendix (Figures 16 – 19). In addition, a nested calibration curve was created using fifteen PFOA standard solutions within a

concentration range of 0.150 – 6000 nM. The nested calibration curve of the PFOA standards was plotted and fitted with a best-fit line using 1/x weight, and is shown in Figure 8.

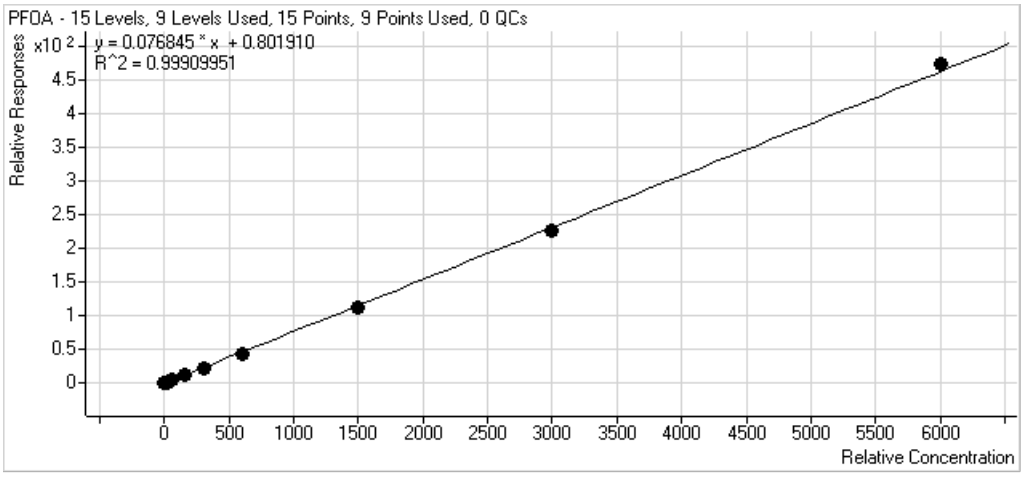

Figure 8. A nested calibration curve created from 0.150 – 6000 nM PFOA standards using method 1. Agilent MassHunter Quantitative software was used to fit the nested calibration curve using 1/x weight, and the best-fit line is displayed on the plot.

Using method 2 (using the Higgins Sprite C_{18} column), the retention time for PFOA was 3.665 min, and a 6-μM standard yielded a peak area of 4.68×10^6 counts•min; the TIC MRM chromatogram for this standard is shown in Figure 9.

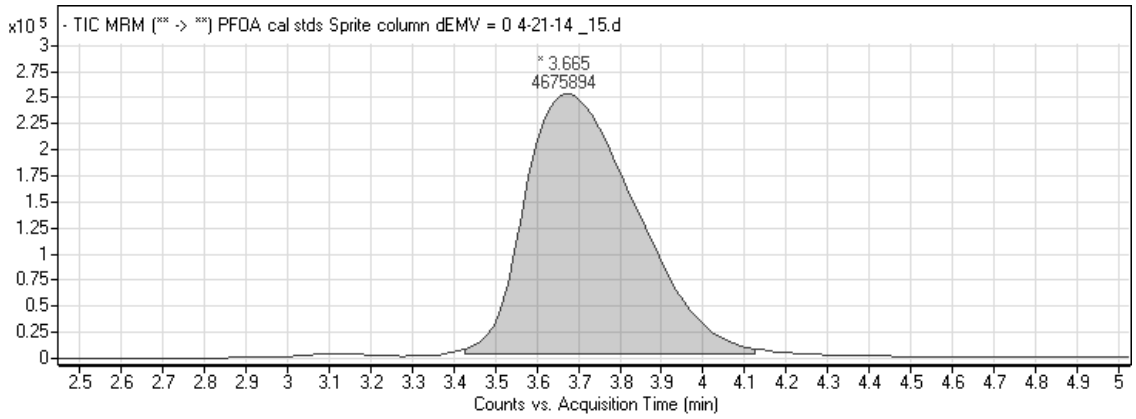

Figure 9. The TIC MRM chromatogram of 6 μM PFOA obtained using method 2. PFOA has a retention time of 3.665 min and a peak area of 4.68×10^6 counts•min.

Using Agilent's MassHunter Qualitative software, the MRM transition chromatograms were extracted from the 6-μM PFOA TIC chromatogram that was obtained using method 2. The MRM transitions include 413 → 369, 413 → 219, 413 → 169, and 413 → 119 *m/z* for PFOA and 417 → 372 *m/z* for [$^{13}C_4$]-PFOA (internal standard); these MRM chromatograms are displayed in the Appendix (Figures 20 – 24). In addition, a nested calibration curve was created using fifteen PFOA standard solutions within a concentration range of 0.150 – 6000 nM. The nested calibration curve of the PFOA standards was plotted and fitted with a best-fit line using 1/x weight, and is shown in Figure 10.

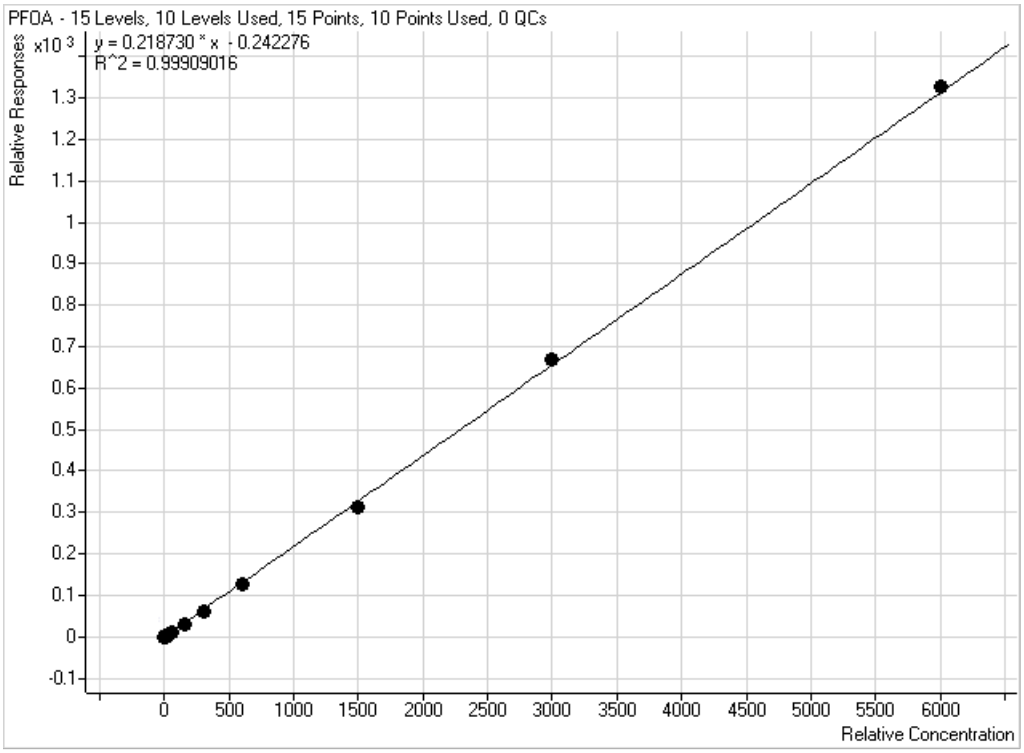

Figure 10. A nested calibration curve created from 0.150 – 6000 nM PFOA standards using method 2. Agilent MassHunter Quantitative software was used to fit the nested calibration curve using 1/x weight, and the best-fit line is displayed on the plot.

Using method 3 (using the Agilent Eclipse C_{18} column), the retention time for PFOA was 3.088 min, and a 6-μM standard yielded a peak area of 2.14×10^7 counts•min; the TIC MRM chromatogram is shown in Figure 11.

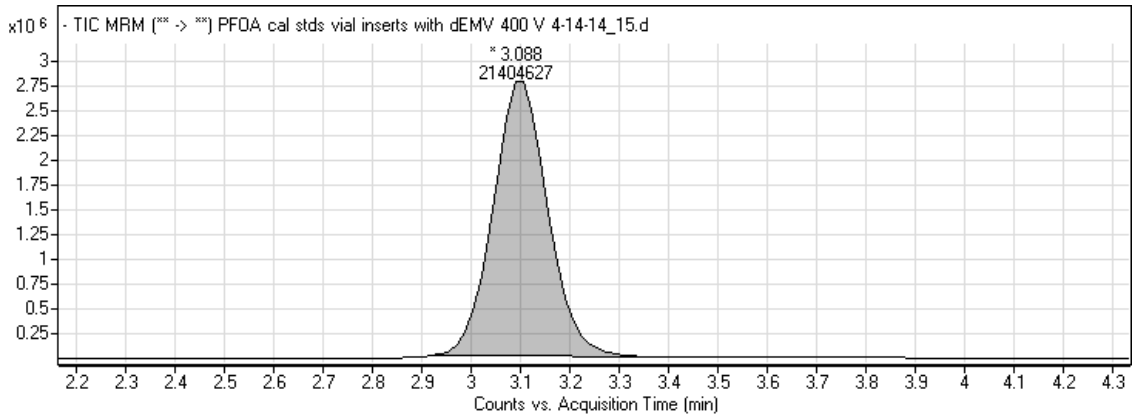

Figure 11. The TIC MRM chromatogram of 6 μM PFOA obtained using method 3. PFOA has a retention time of 3.088 min and a peak area of 2.14×10^7 counts•min.

Using Agilent's MassHunter Qualitative software, the MRM transition chromatograms were extracted from the 6-μM PFOA TIC chromatogram that was obtained using method 3. The MRM transitions include 413 → 369, 413 → 219, 413 → 169, and 413 → 119 *m/z* for PFOA and 417 → 372 *m/z* for [$^{13}C_4$]-PFOA (internal standard); these MRM chromatograms are displayed in the Appendix (Figures 25 – 29). In addition, a nested calibration curve was created using fifteen PFOA standard solutions within a concentration range of 0.150 – 6000 nM. The nested calibration curve of the PFOA standards was plotted and fitted with a best-fit line using 1/x weight, and is shown in Figure 12.

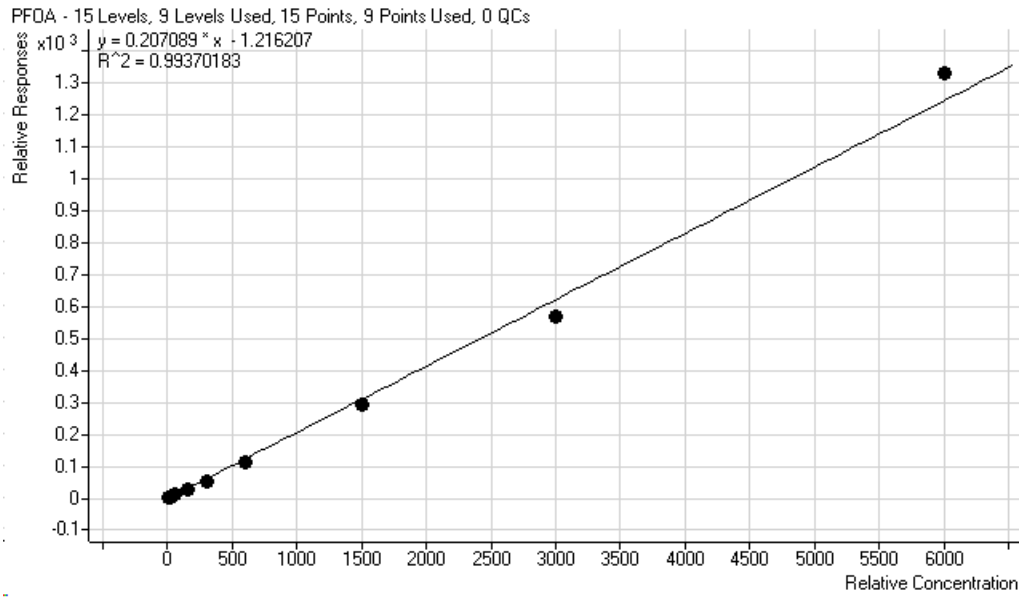

Figure 12. A nested calibration curve created from 0.150 – 6000 nM PFOA standards using method 3. Agilent MassHunter Quantitative software was used to fit the nested calibration curve using 1/x weight, and the best-fit line is displayed on the plot.

ii. Equilibration time determination

The time of complete equilibration for HSA and PFOA using equilibrium dialysis was successfully determined to be 120 hours (5 days) at room temperature. This time of equilibration was determined by making an equilibration time plot, in which percent PFOA bound to HSA was plotted as a function of time (in hours); the equilibration time plot for PFOA and HSA using equilibrium dialysis is shown in Figure 13. The timepoints tested were 18, 24, 48, 72, 86, 96, and 120 hours of equilibration. At 48 hours, the percentage of bound PFOA to HSA was 98.6%; thus, all equilibrium dialysis experiments were carried out over a 48-hour timespan since a significant amount (~99%) of PFOA was bound to HSA at this time point. This was a reasonable compromise since the bound

percentage difference between the 48- and 120-hour timepoints was negligible and since 120 hours is too long for experimental purposes.

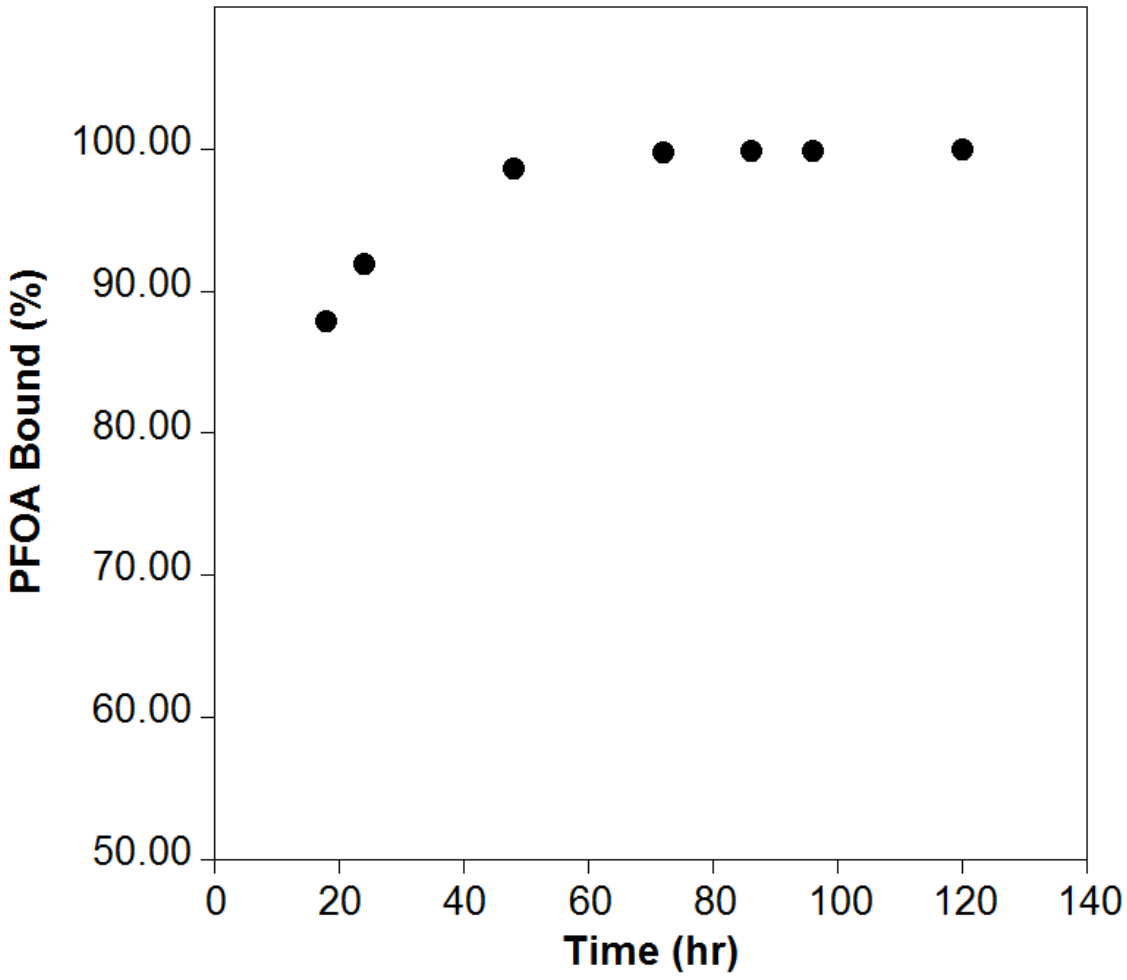

Figure 13. The equilibration time plot used to determine the time of equilibration for PFOA and HSA using equilibrium dialysis. The timepoints tested were 18, 24, 48, 72, 86, 96, and 120 hours of equilibration.

Furthermore, the times of equilibration for perfluorobutanoic acid (PFBA) and perfluorododecanoic acid (PFDoA) with HSA using equilibrium dialysis were

determined to be 120 hr, with no significant difference between the 96 hr and the 120 hr timepoints, as shown in Table 5. However, due to the overall similarity to PFOA in terms of percent bound at each timepoint, it is reasonable to assume that 48 hours would be a suitable equilibration time for PFBA and PFDoA.

Table 5. The percent bound to HSA, at specific time points, for PFBA, PFOA, and PFDoA, determined by equilibrium dialysis and LC-MS/MS.

PFAA	Timepoint (hr)	Percent Bound to HSA
PFBA	96	99.1%
	120	98.6%
PFOA	96	99.9%
	120	100.0%
PFDoA	96	99.3%
	120	98.2%

iii. HSA-PFOA binding experiments to measure protein-ligand affinity

Binding constants (K_a values) in this study were determined by constructing a binding isotherm and curve-fitting the data by using the appropriate mathematical model. Seventeen PFOA:HSA mole ratios were tested in triplicate, ranging from 0.01:1 to 16:1, the concentration of HSA was held constant, and the total equilibration time was 48 hours. Accordingly, the binding coefficient ($\overline{\upsilon}$ = $[PFOA]_{bound}/[HSA]$) was plotted as a function of free PFOA concentration. The resulting binding isotherm data were fitted using two different mathematical models. In the first model, it was assumed that there was only one class of binding sites available in HSA for PFOA to bind, and so the plot was subsequently modeled by using equation 7 in KaleidaGraph. The resulting binding isotherm is shown in Figure 14.

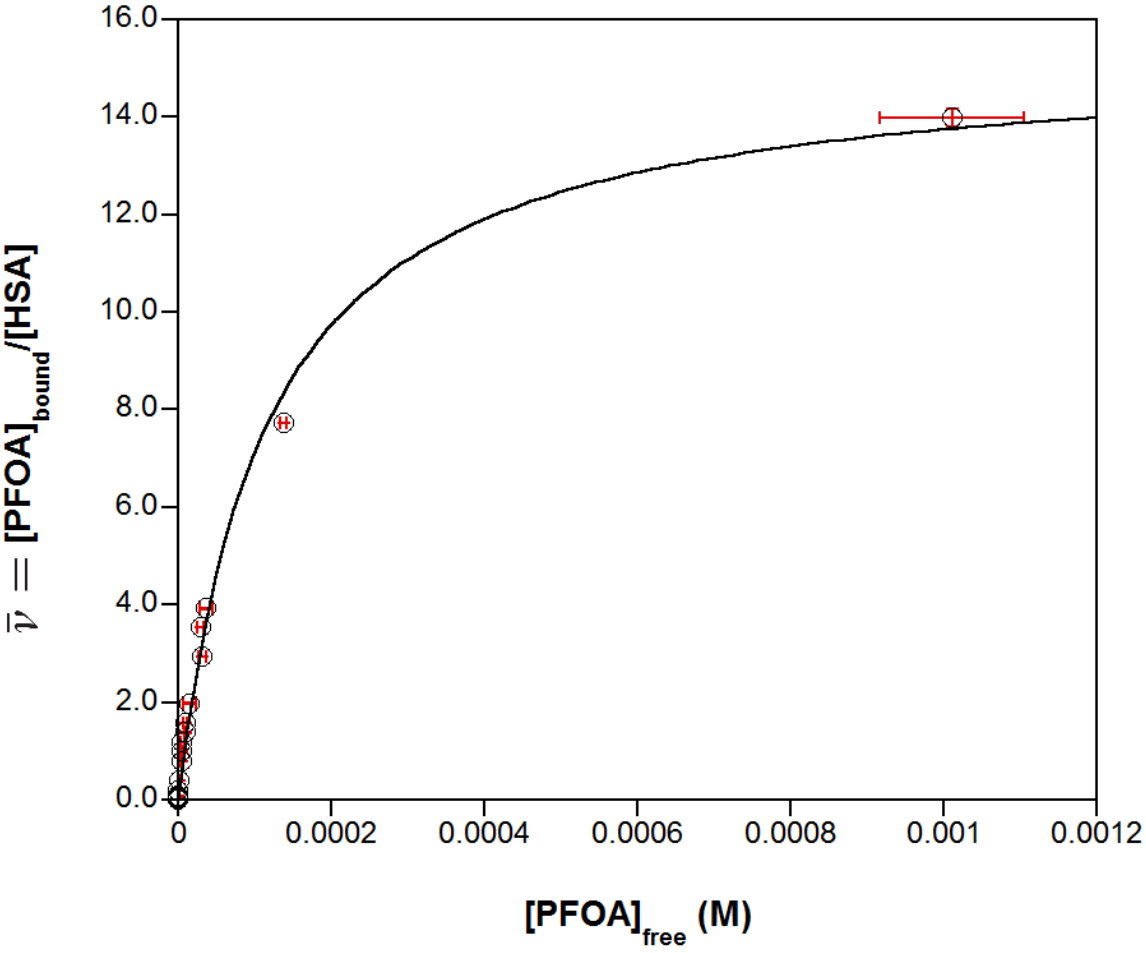

Figure 14. The binding coefficient, $\bar{\upsilon}$, for the binding of PFOA to 500 µM HSA versus free concentration of PFOA ($[PFOA]_{free}$). This binding isotherm was fitted using the one-binding class model (equation 7); the best-fit parameters for this curve are K_a = 8.7 (± 0.6) x 10^3 M^{-1} and n = 15.3 (± 0.4) sites, and the R^2 value for this fit is 0.9930. Error bars (both x and y) represent standard deviations from triplicate measurements.

The corresponding best-fit parameters for the one-binding class fit in Figure 14 are summarized in Table 6. In summary, the one-binding class model demonstrated that there are approximately 15 binding sites in HSA that are associated with a binding

constant that is on the order of 10^3 M^{-1}. However, this binding constant did not agree well with the literature values for PFOA-serum albumin binding constants listed in Table 1, which typically range between $10^4 – 10^6$ M^{-1}. Consequently, a two-binding class model was sought to determine if more reasonable binding constants could be obtained.

The PFOA-HSA binding isotherm data were fitted using a mathematical model that assumed that there are two binding site classes in HSA (two-binding class model; equation 8). The resulting fitted plot is displayed in Figure 15.

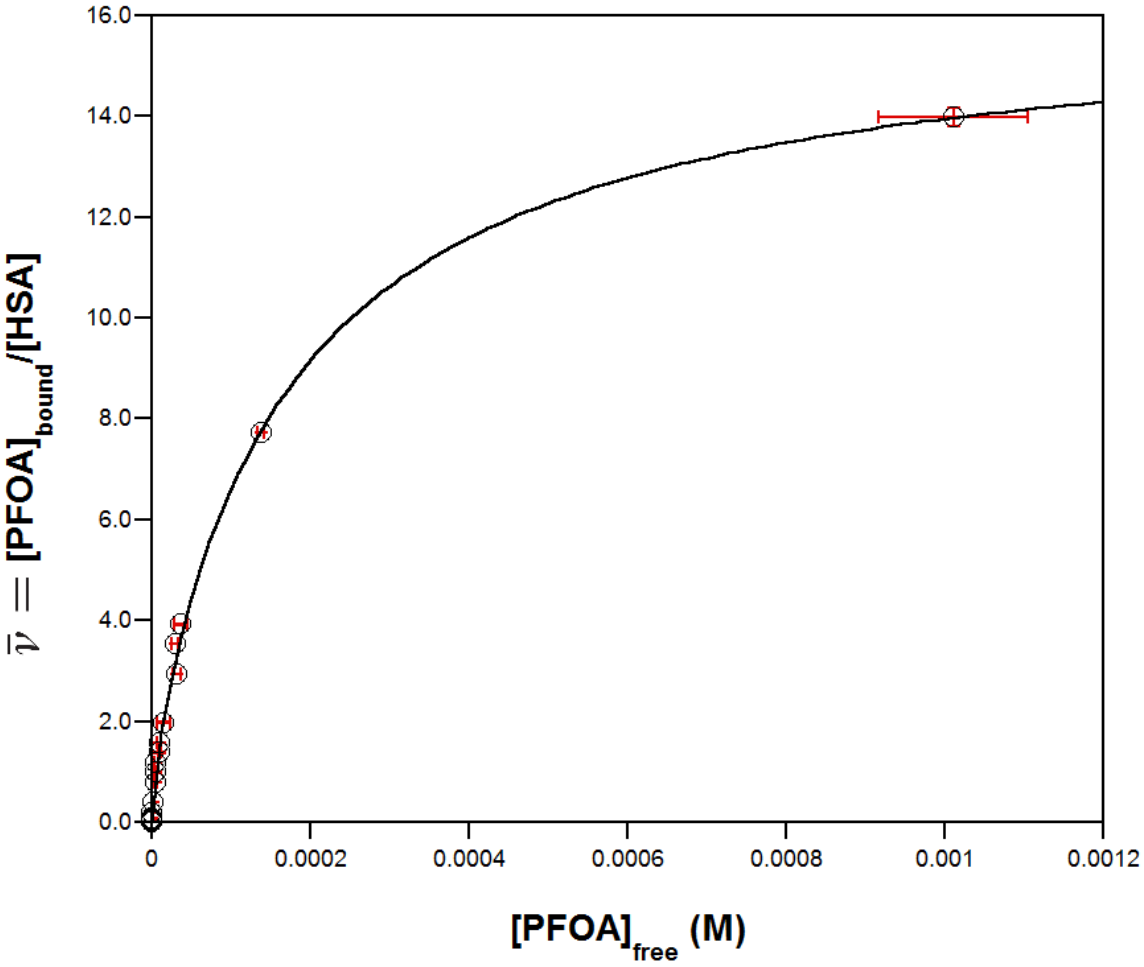

Figure 15. The binding coefficient, $\bar{\upsilon}$, for the binding of PFOA to 500 μM HSA versus free concentration of PFOA ($[PFOA]_{free}$). This binding isotherm was fitted using the two-binding class model (equation 8); the best-fit parameters for this curve are $K_{a,1}$ = 1.1 (± 0.9) x 10^5 M^{-1}, n_1 = 1.5 (± 0.8) sites, $K_{a,2}$ = 5.5 (± 0.9) x 10^3 M^{-1}, and n_2 = 15.3 (± 0.4) sites, and the R^2 value for this fit is 0.9979. Error bars (both x and y) represent standard deviations from triplicate measurements.

The corresponding the best-fit parameters for Figure 15 are summarized in Table 6. According to the two-binding class model, there is one binding site in HSA that

has a high affinity for PFOA ($K_{a,1} \sim 10^5$ M^{-1}) as well as 15 other binding sites that are associated with a weaker affinity ($K_{a,2} \sim 10^3$ M^{-1}).

Table 6. The corresponding K_a, n, and R^2 values for the HSA-PFOA binding isotherm plots, fitted using the one- and two-binding class models (Figures 14 and 15).

One-binding class model		**Two-binding class model**	
$\boldsymbol{K_a}$ **(M^{-1})**	8.7 (± 0.6) × 10^3	$\boldsymbol{K_{a,1}}$ **(M^{-1})**	1.1 (± 0.9) × 10^5
$\boldsymbol{n}$	15.3 (± 0.4)	$\boldsymbol{n_1}$	1.5 (± 0.8)
$\boldsymbol{R^2}$	0.9930	$\boldsymbol{K_{a,2}}$ **(M^{-1})**	5.5 (± 0.9) × 10^3
		$\boldsymbol{n_2}$	14.7 (± 0.6)
		$\boldsymbol{R^2}$	0.9979

The results from the two-binding class model are significant in that: (1) the $K_{a,1}$ binding constant agrees better with the values reported in the literature for PFOA-serum albumin binding, the majority of which range on the order of 10^4 to 10^5 M^{-1};[23, 25, 26, 28, 41, 43] (2) the two binding class model is visually a better fit of the HSA-PFOA binding isotherm data, and quantitatively, it has a higher R^2 value of 0.9979; and (3) the differences in the $K_{a,1}$ and $K_{a,2}$ values may provide clues about the mechanisms of binding of PFOA to HSA.

As shown in Table 1, the literature values of the binding constants for PFOA-serum albumin typically range from 10^4 to 10^5 M^{-1},[23, 25, 26, 28, 41, 43] and the $K_{a,1}$ binding constant obtained from the two-binding class model (which is on the order of 10^5 M^{-1}) agrees with this range of literature values. This better agreement with the literature values suggests that the two-binding class model is a more accurate representation of the HSA-PFOA system. Furthermore, the better curve fit of the data in Figure 9 as well as its higher R^2 value further support the idea that the two-binding class model better represents

the HSA-PFOA system. Moreover, the smaller K_a value obtained when using the one-binding class model reflects the fact that it is is a weighted average of the two binding constants from the two-binding class model. In the two-binding class model, since there are more binding sites ($n_2 \approx 15$ sites) associated with the weaker binding affinity ($K_{a,2}$), the weaker affinity is more heavily weighted in the one-binding class model. This explains why the one-binding class model K_a value is on the same order of magnitude of $K_{a,2}$ from the two-binding class model.

Furthermore, the affinity differences between the $K_{a,1}$ and $K_{a,2}$ values obtained from the two-binding class model may provide mechanistic information on HSA-PFOA binding. According to the two-binding class model, there are approximately two high-affinity binding sites, which are on the order of 10^5 M^{-1}, for PFOA, as well as approximately 15 lower-affinity sites for PFOA. Since physiologically-relevant concentrations are those in which the PFOA:HSA mole ratio is low, then it is likely that the high-affinity binding sites would be occupied under such conditions. Using the same logic, the lower-affinity binding sites will be more likely to be occupied at a high PFOA:HSA mole ratio, which is an unrealistic scenario. However, since HSA binds to a variety of endogenous and exogenous ligands, including fatty acids,[35, 38-40] then it is possible that PFOA can bind to a lower-affinity binding site in HSA if the other binding sites are occupied by other ligands at a low PFOA:HSA mole ratio. For this reason, binding competitive experiments between PFAAs and fatty acids must be carried out in order to gain insight into the mechanism of binding of PFAAs to HSA under physiologically relevant conditions. Since there is only one binding site (n_1) associated

with $K_{a,1}$, then the first molecule of PFOA to bind to HSA will bind with that affinity, whereas subsequent PFOA molecules will bind with a lower affinity ($K_{a,2}$).

The data obtained in this study can be further examined via comparisons to published reports that also analyzed the binding mechanism of certain PFAAs to HSA. The first study utilized molecular modeling to investigate the binding thermodynamics and binding sites of PFOA to HSA,[55] while the second study provided and analyzed the crystal structure of HSA with bound perfluorooctane sulfonate (PFOS).[56]

In the first study, Salvalaglio *et al*.,[55] using computational methods, determined that the maximum number of PFOA molecules that can bind to HSA was nine, and that there were only five stable PFOA-HSA complexes. Of the five theoretically stable complexes, only two complexes had a very large probability of stability: complexes J and T. Complex J overlaps with fatty acid site 8, and is located in the core of the protein between domains II and III of HSA, and is the most stable complex according to Salvalaglio *et al*. In this complex, the fluorinated tail of PFOA exhibits van der Waals interactions with Lys 199, Lys 195, Arg 218, Arg 222, and Trp 214. Furthermore, electrostatic interactions between the carboxylate head group of PFOA and charged residues are present and contribute to the overall stability of complex J. Complex T coincides with fatty acid site 1, which is a favorable binding site for short chain fatty acids. In this complex, the polar carboxylate head group of PFOA interacts with Arg 117 and Arg 186, while the nonpolar fluorinated tail of PFOA interacts with a network of aromatic and nonpolar groups from Tyr 138, Tyr 161, Ile 142, His 146, Phe 149, Phe 157, Leu 182, and Leu 185.[55]

The computational data from Salvalaglio *et al*. might be in agreement with our observed data. Specifically, the high probability of two stable HSA-PFOA complexes J and T, as shown by Salvalaglio *et al*., corresponds to our two-binding class model, in which we have shown that there are approximately two higher-affinity PFOA binding sites in HSA, compared to the fifteen lower-affinity sites, under physiological concentrations. Thus, the computational results from Salvalaglio *et al*. and the data from our study seem to suggest that there are two binding sites in HSA that exhibit favorable and high-affinity interactions with PFOA, as well as some number of lower-affinity binding sites.

In the second study, Luo *et al*.[56] obtained a crystal structure of HSA with bound PFOS. According to their crystal structure, there are two PFOS ligands bound to HSA, with one bound to subdomain IIIA (which overlaps with fatty acid binding sites 3/4) and the other ligand bound at the interface of subdomains IIA and IIB (which coincides with fatty acid binding site 6). In general, the authors observed that the polar sulfonate head group of PFOS interacts with hydrophilic amino acids in HSA, while the fluorinated tail of PFOS interacts with adjacent hydrophobic residues. Moreover, the authors successfully demonstrated that the HSA-PFOS complex is more compact than the unliganded HSA structure, which contrasts with the conformational changes induced by fatty acids in HSA, which exhibits a less compact structure.[56] Although we cannot directly compare our data with this study since we did not study the binding interactions between PFOS and HSA or utilize X-ray crystallography, it is interesting to point out that the crystal structure demonstrated that PFOS binds to HSA at a 2:1 mole ratio, while our data demonstrated that there are two high-affinity binding sites in HSA for PFOA.

Altogether, the computational data by Salvalaglio *et al*.,[55] the crystal structure data by Luo *et al*.,[56] and our data all suggest that PFOA binds to HSA at a 2:1 mole ratio (at two high affinity binding sites). Although the data by Salvalaglio *et al*. is theoretical and the results from Luo *et al*. involve a different method and ligand (albeit structurally similar to PFOA), the results from these two studies correspond well to our data obtained from equilibrium dialysis and LC-MS/MS. In addition, studies from Chen *et al*.,[23] MacManus-Spencer *et al*.,[26] and Messina *et al*.[43] also obtained a binding constant of 10^5 M^{-1} for serum albumin-PFOA binding (see Table 1). Therefore, this excellent agreement with published studies demonstrates that our equilibrium dialysis and LC-MS/MS method is a valid way to measure binding constants, as well as the number of binding sites, between HSA and PFAAs.

4. Conclusions

We have demonstrated that the use of an improved, higher-throughput equilibrium dialysis method coupled with LC-MS/MS quantitation is a viable method to determine binding constants between HSA and PFOA, which provided data that was comparable to the literature. Using a two-binding class model, it was determined that there are two higher-affinity binding sites in HSA for PFOA that would be more likely to be occupied under physiological conditions. This result corresponded well with the literature values,[23, 26, 43] as well as to two mechanistic studies which demonstrated that PFOA and PFOS bind to HSA at a 2:1 molar ratio.[55, 56] In the future, a more complete and deeper understanding of the binding mechanism of PFOA to HSA may be obtained by acquiring a crystal structure of HSA with bound PFOA, in conjunction with more

binding experiments between other PFAAs and HSA achieved via equilibrium dialysis. Furthermore, the equilibrium dialysis and LC-MS/MS methods that we developed in this study can be applied to investigate the binding of PFAAs to HSA under varying solution conditions (i.e., pH and ionic strength), the binding of PFAAs to other physiologically relevant proteins, such as hemoglobin and myoglobin, to aid in the effort of furthering our understanding of the toxicokinetics and bioaccumulation patterns of PFAAs in humans.

5. Future Work

In this project, there are a plethora of areas in which the methods developed in this study can be applied to further explore the binding mechanisms of PFFAs to proteins and therefore their toxicokinetics in organisms, including:

- Investigating the binding of various PFAAs to HSA, especially those of shorter chain lengths.
- Probing how solution conditions (including ionic strength and pH) influence the binding of various PFAAs to HSA.
- Measuring the binding constants of various PFAAs to other physiologically relevant proteins, including hemoglobin and myoglobin.
- Examining the competitive binding between PFAAs and fatty acids for HSA.
- Growing crystals of HSA (and of other proteins) with bound PFAAs to examine conformational changes via X-ray crystallography.
- Studying the binding of PFAAs to HSA (and to other proteins) under controlled, physiological temperatures.

In addition, the examination of crystal structures of HSA bound with PFAAs may further elucidate the subtle conformational changes that occur upon binding, thereby furthering our understanding of the binding mechanisms of PFAAs to HSA.

6. References

1. Schultz, M. M.; Barofsky, D. F.; Field, J. A. Fluorinated alkyl surfactants. *Environ. Eng. Sci.* **2003**, *20,* 487-501.
2. Lau, C.; Anitole, K.; Hodes, C.; Lai, D.; Pfahles-Hutchens, A.; Seed, J. Perfluoroalkyl acids: A review of monitoring and toxicological findings. *Toxicol. Sci.* **2007**, *99*, 366-394.
3. Andersen, M. E.; Butenhoff, J. L.; Chang, S.; Farrar, D. G.; Kennedy, G. L.; Lau, C.; Olsen, G. W.; Seed, J.; Wallace, K. B. Perfluoroalkyl acids and related chemistries - toxicokinetics and modes of action. *Toxicol*. *Sci*. **2008**, *102*, 3-14.
4. Ritter, S. K. Fluorochemicals go short. *Chem. Eng. News* **2010**, *88*, 12-17.
5. Graham Solomons, T.W.; Fryhle, C.B. *Organic Chemistry*. 10th Ed; John Wiley & Sons, Inc.: Hoboken, **2011**. Page 462.
6. Rayne, S.; Forest, K. Theoretical studies on the pK_a values of perfluoroalkyl carboxylic acids. *J. Mol. Struc.-THEOCHEM*. **2010**, *949*, 60-69.
7. Cheng, J.; Psillakis, E; Hoffmann, M. R.; Colussi, A. J. Acid dissociation versus molecular association of perfluoroalkyl oxoacids: Environmental implications. *J. Phys. Chem. A*. **2009**, *113*, 8152–8156.

8. Olsen, G.; Ehresman, D.; Froehlich, J.; Burris, J.; Butenhoff, J. Evaluation of the half-life ($t_{1/2}$) of elimination of perfluorooctanesulfonate (PFOS), perfluorohexanesulfonate (PFHS) and perfluorooctanoate (PFOA) from human serum. *FLUOROS.* **2005**, *18–20*, 1. Available at: http://www.chem.utoronto.ca/symposium/fluoros/pdfs/TOX017Olsen.pdf. Accessed December 18, 2013.
9. Johnson, J. D.; Gibson, S. J.; Ober, R. E. Extent and route of excretion and tissue distribution of total carbon-14 in rats after a single I.V. dose of FC-95-14C. **1979**, Riker Laboratories, Inc., St Paul, MN. US EPA Administrative Record, 8EHQ-1180-00374.
10. Kemper, R. A. Perfluorooctanoic acid: Toxicokinetics in the rat. **2003**, DuPont Haskell Laboratories, Project No. DuPont–7473. US EPA Administrative Record, AR-226-1499.
11. Lemal, D. M. Perspective on fluorocarbon chemistry. *J. Org. Chem*. **2004**, *69*, 1-11.
12. Houde, M.; Martin, J.; Letcher, R.; Solomon, K.; Muir, D. Biological monitoring of polyfluoroalkyl substances: A review. *Environ. Sci. Technol*. **2006**, *40*, 3463-3473.
13. Shi, Y.; Wang, J.; Pan, Y.; Cai, Y. Tissue distribution of perfluorinated compounds in farmed freshwater fish and human exposure by consumption. *Environ. Toxicol. Chem*. **2012**, *31*, 717-723.
14. Taniyasu, S.; Kannan, K.; Horii, Y.; Hanari, N.; Yamashita, N. A survey of perfluorooctane sulfonate and related perfluorinated organic compounds in water, fish, birds, and humans from Japan. *Environ. Sci. Technol*. **2003**, *37*, 2634-2639.

15. Ankley, G.; Kuehl, D.; Kahl, M.; Jensen, K.; Linnum, A.; Leino, R.; Villeneuve, D. Reproductive and developmental toxicity and bioconcentration of perfluorooctanesulfonate in a partial life-cycle test with the fathead minnow (Pimephales promelas). *Environ. Toxicol. Chem*. **2005**, *24*, 2316-2324.

16. Kelly, B. C.; Ikonomou, M. G.; Blair, J. D.; Surridge, B.; Hoover, D.; Grace, R.; Gobas, F. A. P. C. Perfluoroalkyl contaminants in an Arctic marine food web: Trophic magnification and wildlife exposure. *Environ. Sci. Technol*. **2009**, *43*, 4037-4043.

17. Vanden Heuvel, J. P.; Kuslikis, B. I.; Van Rafelghem, M. J.; Peterson, R. E. Tissue distribution, metabolism, and elimination of perfluorooctanoic acid in male and female rats. *J. Biochem. Toxicol.* **1991**, *6,* 83-92.

18. Martin, J. W.; Mabury, S. A.; Solomon, K. R.; Muir, D. C. G. Dietary accumulation of perfluorinated acids in juvenile rainbow trout (*Oncorhynchus mykiss*). *Environ. Toxicol. Chem.* **2003**, *22,* 189-195.

19. Verreault, J.; Houde, M.; Gabrielsen, G. W.; Berger, U.; Haukås, M.; Letcher, R. J.; Muir, D. C. G. Perfluorinated alkyl substances in plasma, liver, brain, and eggs of glaucous gulls (*Larus hyperboreus*) from the Norwegian Arctic. *Environ. Sci. Technol*. **2005**, *39*, 7439-7445.

20. Ahrens, L.; Siebert, U.; Ebinghaus, R. Total body burden and tissue distribution of polyfluorinated compounds in harbor seals (*Phoca vitulina*) from the German Bight. *Mar. Pollut. Bull*. **2009**, *58*, 520-525.

21. Yoo, H.; Guruge, K. S.; Yamanaka, N.; Sato, C.; Mikami, O.; Miyazaki, S.; Yamashita, N.; Giesy, J. P. Depuration kinetics and tissue disposition of PFOA and PFOS in white leghorn chickens (*Gallus gallus*) administered by subcutaneous implantation. *Ecotox. Environ. Safe*. **2009**, *72*, 26-36.

22. Vestergren, R.; Cousins, I. T. Tracking the pathways of human exposure to perfluorocarboxylates. *Environ. Sci. Technol*. **2009**, *43*, 5565-5575.

23. Chen, Y.; Guo, L. Fluorescence study on site-specific binding of perfluoroalkyl acids to human serum albumin. *Arch. Toxicol*. **2009**, *83*, 255-261.

24. Bischel, H. N.; MacManus-Spencer, L. A.; Luthy, R. G. Noncovalent interactions of long-chain perfluoroalkyl acids with serum albumin. *Environ. Sci. Technol.* **2010**, *44,* 5263-5269.

25. Hebert, P. C.; MacManus-Spencer, L. A. Development of a fluorescence model for the binding of medium- to long-chain perfluoroalkyl acids to human serum albumin through a mechanistic evaluation of spectroscopic evidence. *Anal. Chem.* **2010**, *82,* 6463-6471.

26. MacManus-Spencer, L. A.; Tse, M. L.; Hebert, P. C.; Bischel, H. N.; Luthy, R. G. Binding of perfluorocarboxylates to serum albumin: A comparison of analytical methods. *Anal. Chem.* **2010**, *82,* 974-981.

27. Bischel, H. N.; MacManus-Spencer, L. A.; Zhang, C.; Luthy, R. G. Strong associations of short-chain perfluoroalkyl acids with serum albumin and investigation of binding mechanisms. *Environ. Toxicol. Chem.* **2011**, *30,* 2423-2430.

28. O'Connor, M. P.; MacManus-Spencer, L. A. Investigation of the mechanism of binding of medium- and long-chain perfluoroalkyl acids to human serum albumin using fluorescence spectroscopy. *In preparation*.

29. Han, X.; Yang, C.-H.; Snajdr, S. I.; Nabb, D. L.; Mingoia, R. T. Uptake of perfluorooctanoate in freshly isolated hepatocytes from male and female rats. *Toxicol. Lett*. **2008**, *181*, 81-86.

30. Yang, C.-H.; Glover, K. P.; Han, X. Characterization of cellular uptake of perfluorooctanoate via organic anion-transporting polypeptide 1A2, organic anion transporter 4, and urate transporter 1 for their potential roles in mediating human renal reabsorption of perfluorocarboxylates. *Toxicol. Sci*. **2010**, *117*, 294-302.

31. Luebker, D. J.; Hansen, K. J.; Bass, N. M.; Butenhoff, J. L.; Seacat, A. M. Interactions of fluorochemicals with rat liver fatty acid binding protein. *Toxicology* **2002**, *176*, 175-185.

32. Weisiger, R. A. Mechanisms of intracellular fatty acid transport: Role of cytoplasmic-binding proteins. *J. Mol. Neurosci*. **2007**, *33*, 42-44.

33. Hickey, N. J.; Crump, D.; Jones, S. P.; Kennedy, S. W. Effects of 18 perfluoroalkyl compounds on mRNA expression in chicken embryo hepatocyte cultures. *Toxicol. Sci*. **2009**, *111*, 311-320.

34. Carter, D. C. and Ho, J. X. Structure of serum albumin. *Adv. Protein Chem*. **1994**, *45*, 153-203.

35. Putnam, F. W. *The Plasma Proteins*. 2nd Ed; Academic Press, Inc: Orlando, **1984**.

36. Brown, J. R. Structural origins of mammalian albumin. *Fed. Proc*. **1976**, *35*, 2141-2144.

37. Sugio, S.; Kashima, A.; Mochizuki, S.; Noda, M.; Kobayashi, K. Crystal structure of human serum albumin at 2.5 Å resolution. *Protein Eng*. **1999**, *12*, 439-446.

38. Fehske, K. J.; Muller, W. E.; Wollert, U. The location of drug binding sites in human serum albumin. *Biochem. Pharmacol*. **1981**, *30*, 687-692.

39. Kragh-Hansen, U. Molecular aspects of ligand binding to serum albumin. *Pharmacol. Rev*. **1981**, *33*, 17-53.

40. Peters, T. Serum albumin. *Adv. Protein Chem*. **1985**, *37*, 161-245.

41. Wu, L.; Gao, H.; Gao, N.; Chen, F.; Chen, L. Interaction of perfluorooctanoic acid with human serum albumin. *BMC Struct. Biol.* **2009**, *9,* 31.

42. Han, X.; Snow, T. A.; Kemper, R. A.; Jepson, G. W. Binding of perfluorooctanoic acid to rat and human plasma proteins. *Chem. Res. Toxicol.* **2003**, *16,* 775-781.

43. Messina, P.; Prieto, G.; Dodero, V.; Ruso, J. M.; Schulz, P.; Sarmiento, F. Ultraviolet-circular dichroism spectroscopy and potentiometric study of the interaction between human serum albumin and sodium perfluorooctanoate. *Biopolymers* **2005**, *79,* 300-309.

44. Voet, D.; Voet, J. G.; Pratt, C. W. *Fundamentals of Biochemistry: Life at the Molecular Level*. 4th Ed. John Wiley & Sons, Inc.: Hoboken, **2013**.

45. Foy, B.; Frazier, J. Incorporation of protein-binding kinetics and carrier-mediated membrane transport into a model of chemical kinetics in the isolated perfused rat liver. *Toxicol. Mech. Methods* **2003**, *13*, 53-75.

46. Robinson, P.; Rapoport, S. Kinetics of protein-binding determine rates of uptake of drugs by brain. *Am. J. Physiol*. **1986**, *251*, R1212-R1220.

47. Sebille, B.; Zini, R; Madjar, C. V.; Thuaud, N.; Tillement, J. P. Separation procedures used to reveal and follow drug-protein binding. *J Chromatogr*. **1990**, *12*, 51-77.

48. Sebille, B. Methods of drug protein binding determinations. *Fundam Clin Pharmacol*. **1990**, *4*, Suppl 2, 151s-161s.

49. Guide to Equilibrium Dialysis, Harvard Apparatus, 2-9.

50. Kuriyan, J.; Konforti, B.; Wemmer, D. *The Molecules of Life*. 1st Ed. Garland Science: New York, **2012**.

51. Harris, D.C. *Quantitative Chemical Analysis*. 8th Ed. W. H. Freeman and Company: New York, **2010**.

52. Grebe, S. K.; Singh, R. J. LC-MS/MS in the clinical laboratory - where to from here? *Clin Biochem Rev*. **2011**, *32*, 5-31.

53. Last, R.; Jones, D. A.; Shachar-Hill, Y. Towards the plant metabolome and beyond. *Nature* **2007**, *8*, 167-174.

54. Sabin, J.; Prieto, G.; Gonzalez-Perez, A.; Ruso, J. M.; Sarmiento, F. Effects of fluorinated and hydrogenated surfactants on human serum albumin at different pHs. *Biomacromolecules* **2006**, *7,* 176-182.

55. Salvalaglio, M.; Muscionico, I.; Cavallotti, C. Determination of Energies and Sites of Binding of PFOA and PFOS to Human Serum Albumin. *J. Phys. Chem. B* **2010**, *114*, 14860–14874.

56. Luo, Z.; Shi, X.; Hu, Q.; Zhao, B.; Huang, M. Structural Evidence of Perfluorooctane Sulfonate Transport by Human Serum Albumin. *Chem. Res. Toxicol*., **2012**, *25*, 990–992.

7. Appendix

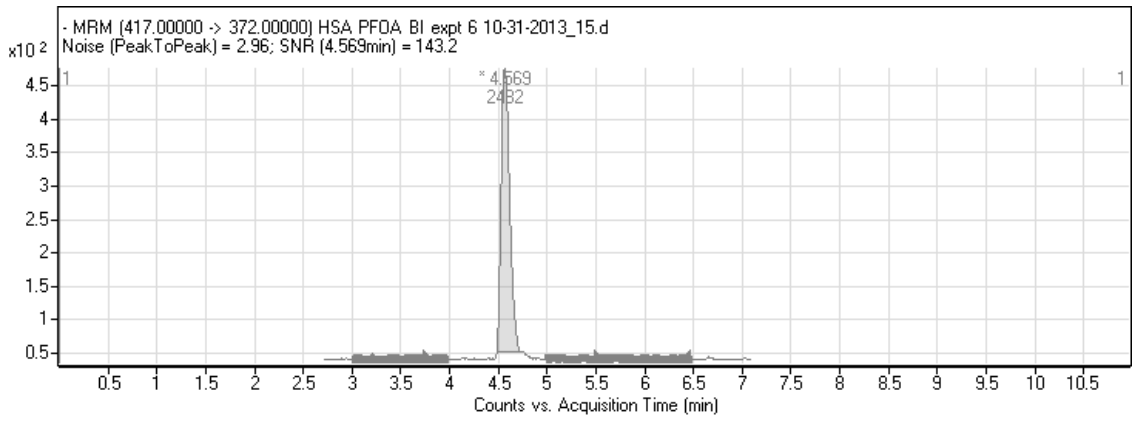

Figure 16. The MRM chromatogram of the 417 → 372 *m/z* transition of 10 nM [$^{13}C_4$]-PFOA obtained from method 1. [$^{13}C_4$]-PFOA has a retention time of 4.569 min, a peak area of 2,482 counts•min, and a signal-to-noise ratio (SNR) of 143.2.

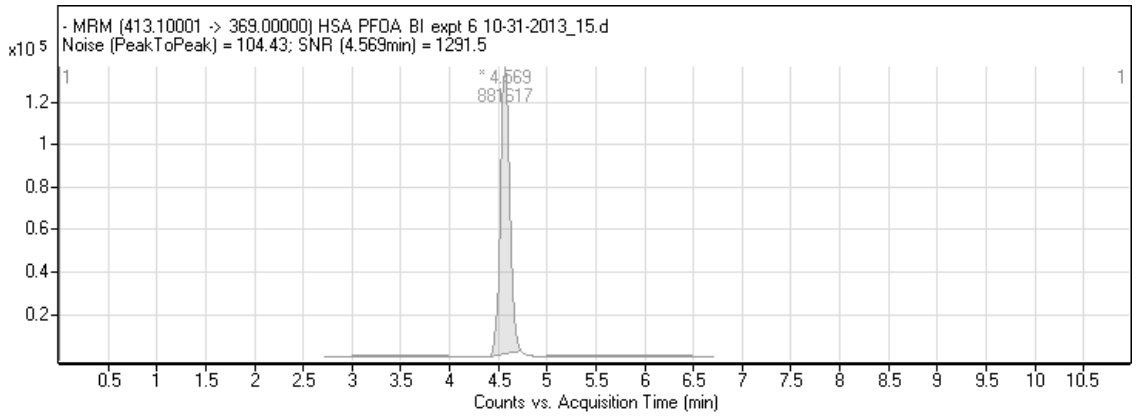

Figure 17. The MRM chromatogram of the 413 → 369 *m/z* transition of 6 μM PFOA obtained from method 1. PFOA has a retention time of 4.569 min, a peak area of 8.82×10^5 counts•min, and a signal-to-noise ratio (SNR) of 1,292.

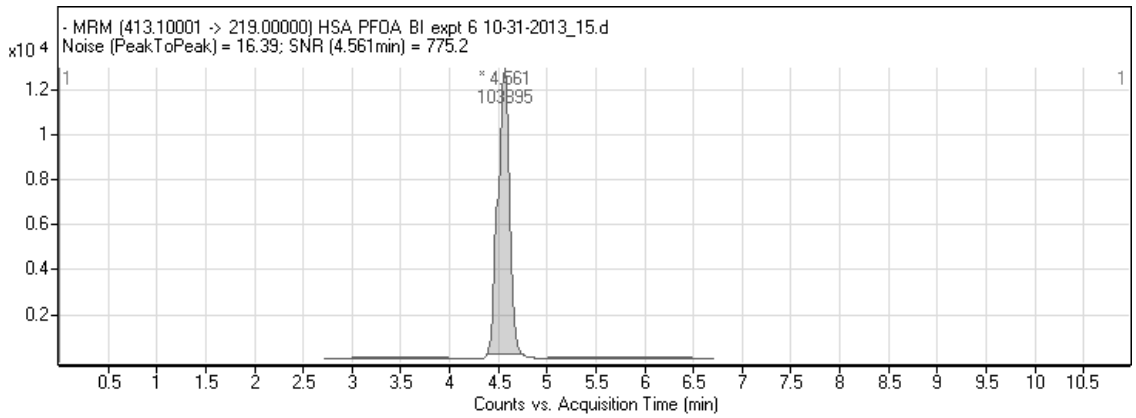

Figure 18. The MRM chromatogram of the 413 → 219 *m/z* transition of 6 μM PFOA obtained from method 1. PFOA has a retention time of 4.561 min, a peak area of 1.04×10^5 counts•min, and a signal-to-noise ratio (SNR) of 775.2.

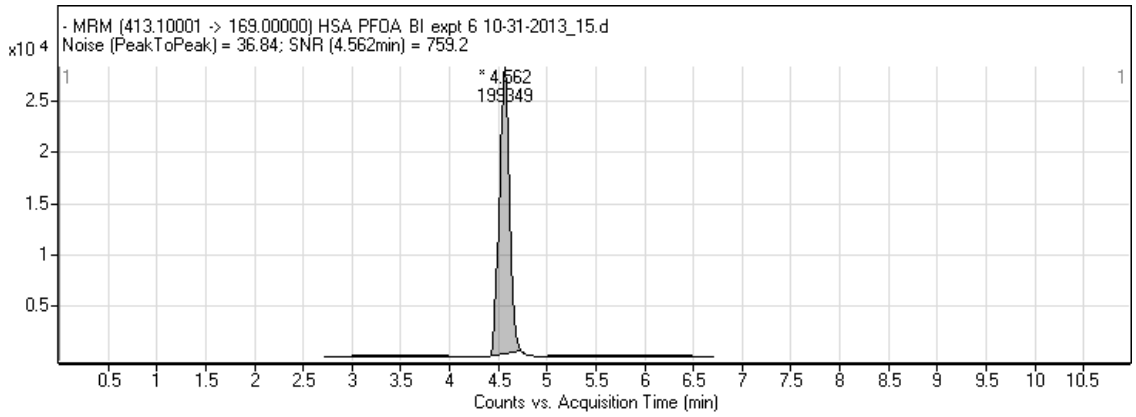

Figure 19. The MRM chromatogram of the 413 → 169 *m/z* transition of 6 μM PFOA obtained from method 1. PFOA has a retention time of 4.562 min, a peak area of 1.99×10^5 counts•min, and a signal-to-noise ratio (SNR) of 759.2.

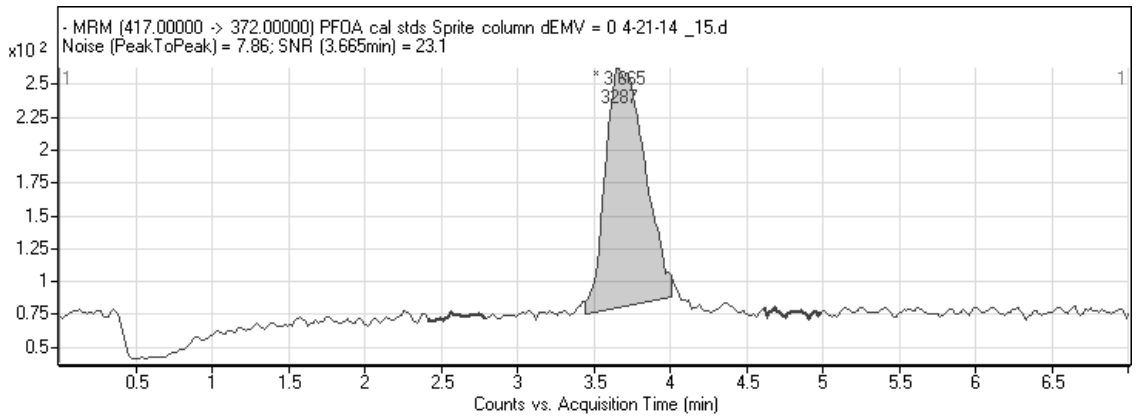

Figure 20. The MRM chromatogram of the 417 → 372 *m/z* transition of 10 nM [$^{13}C_4$]-PFOA obtained from method 2. [$^{13}C_4$]-PFOA has a retention time of 3.665 min, a peak area of 3,287 counts•min, and a signal-to-noise ratio (SNR) of 23.1.

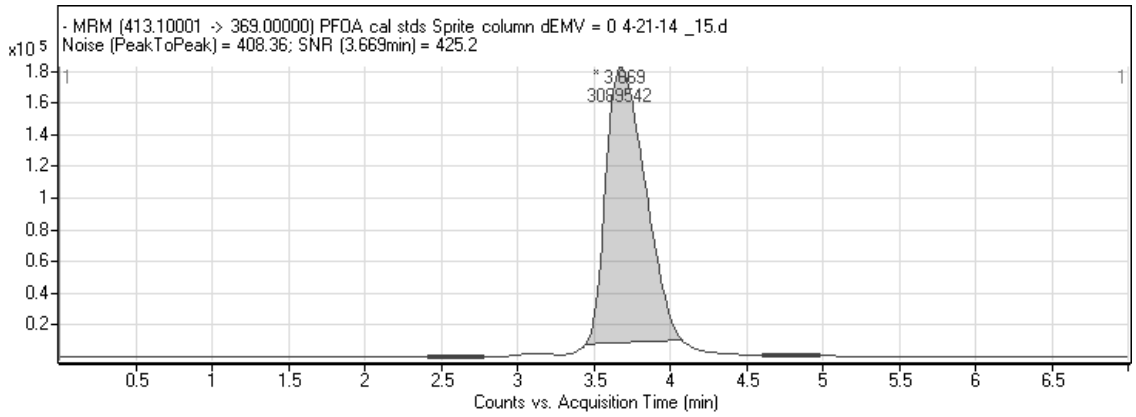

Figure 21 The MRM chromatogram of the 413 → 369 *m/z* transition of 6 μM PFOA obtained from method 2. PFOA has a retention time of 3.669 min, a peak area of 3.09×10^6 counts•min, and a signal-to-noise ratio (SNR) of 425.2.

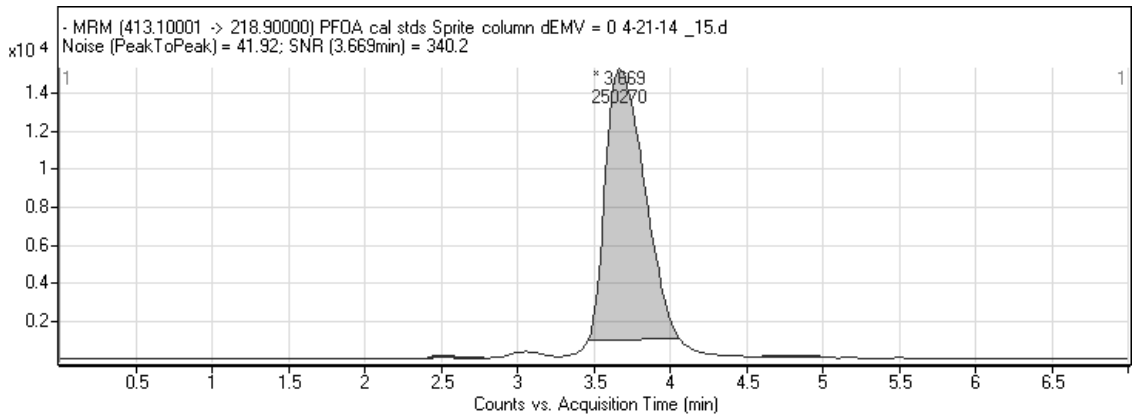

Figure 22. The MRM chromatogram of the 413 → 219 *m/z* transition of 6 μM PFOA obtained from method 2. PFOA has a retention time of 3.669 min, a peak area of 2.50×10^5 counts•min, and a signal-to-noise ratio (SNR) of 340.2.

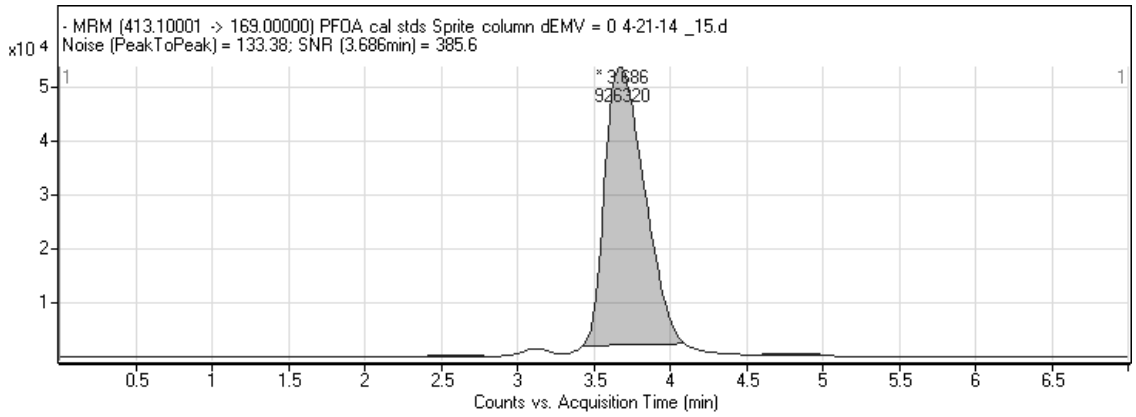

Figure 23. The MRM chromatogram of the 413 → 169 *m/z* transition of 6 μM PFOA obtained from method 2. PFOA has a retention time of 3.686 min, a peak area of 9.26×10^5 counts•min, and a signal-to-noise ratio (SNR) of 385.6.

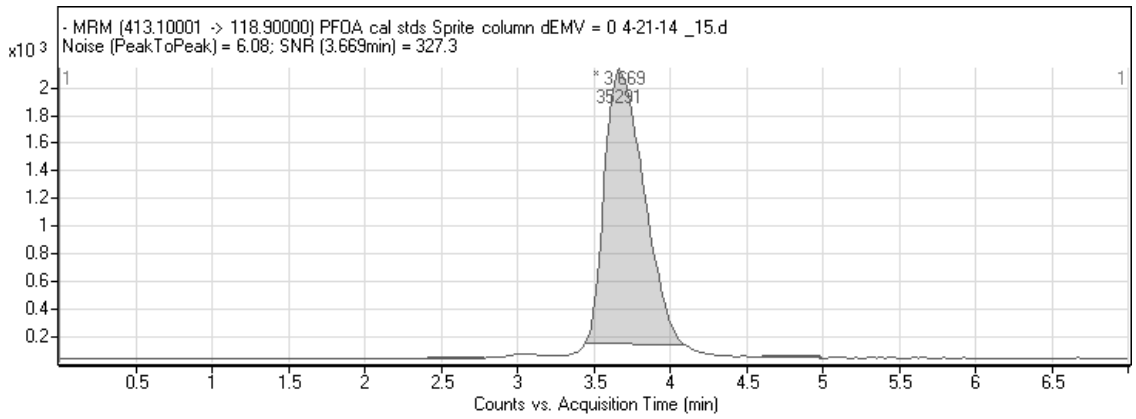

Figure 24. The MRM chromatogram of the 413 → 119 *m/z* transition of 6 μM PFOA obtained from method 2. PFOA has a retention time of 3.669 min, a peak area of 3.53×10^4 counts•min, and a signal-to-noise ratio (SNR) of 327.3.

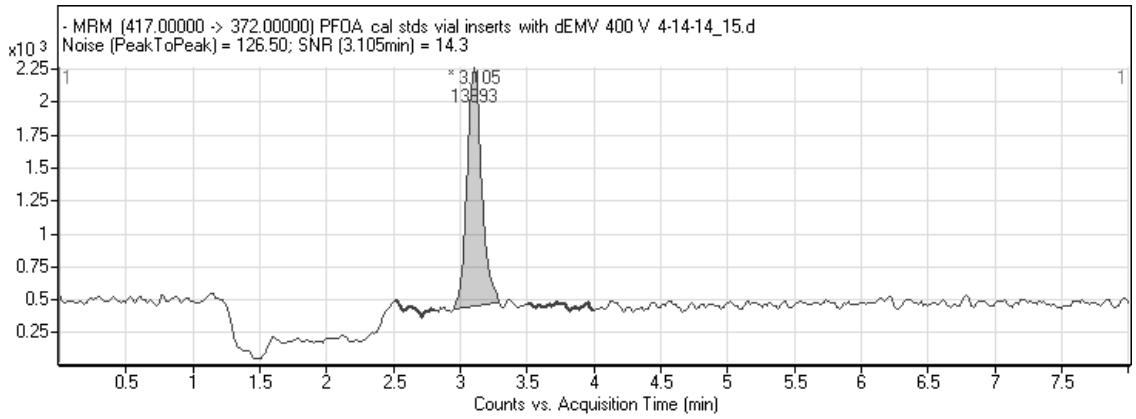

Figure 25. The MRM chromatogram of the 417 → 372 *m/z* transition of 10 nM [$^{13}C_4$]-PFOA obtained from method 3. [$^{13}C_4$]-PFOA has a retention time of 3.105 min, a peak area of 1.39×10^4 counts•min, and a signal-to-noise ratio (SNR) of 14.3.

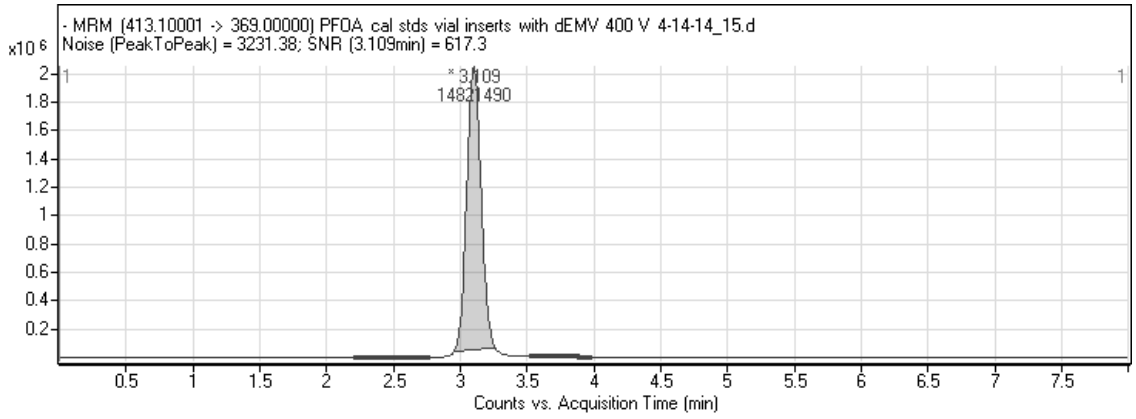

Figure 26. The MRM chromatogram of the 413 → 369 *m/z* transition of 6 μM PFOA obtained from method 3. PFOA has a retention time of 3.109 min, a peak area of 1.48×10^7 counts•min, and a signal-to-noise ratio (SNR) of 617.3.

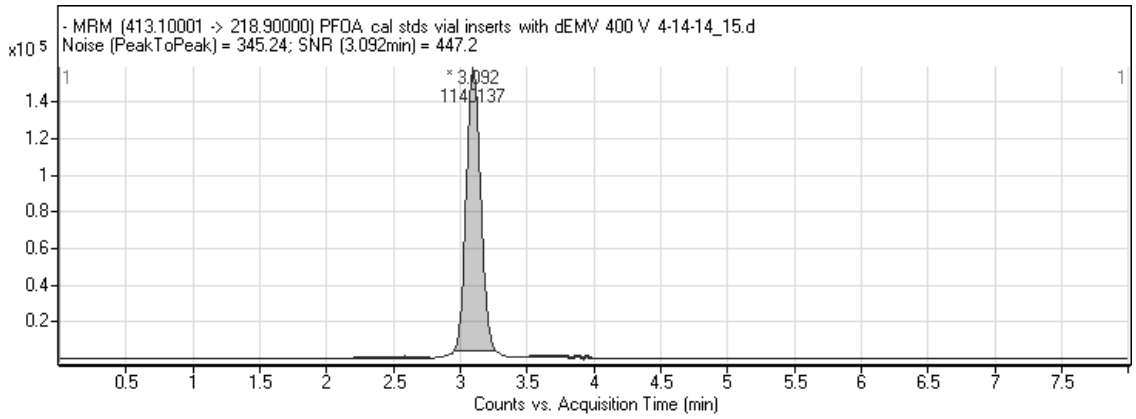

Figure 27. The MRM chromatogram of the 413 → 219 *m/z* transition of 6 μM PFOA obtained from method 3. PFOA has a retention time of 3.092 min, a peak area of 1.14×10^6 counts•min, and a signal-to-noise ratio (SNR) of 447.2.

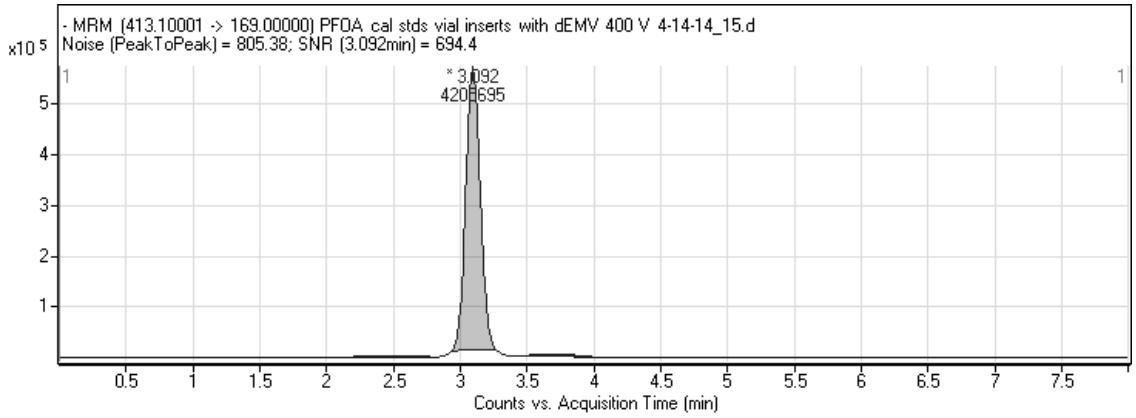

Figure 28. The MRM chromatogram of the 413 → 169 *m/z* transition of 6 μM PFOA obtained from method 3. PFOA has a retention time of 3.092 min, a peak area of 4.21×10^6 counts•min, and a signal-to-noise ratio (SNR) of 694.4.

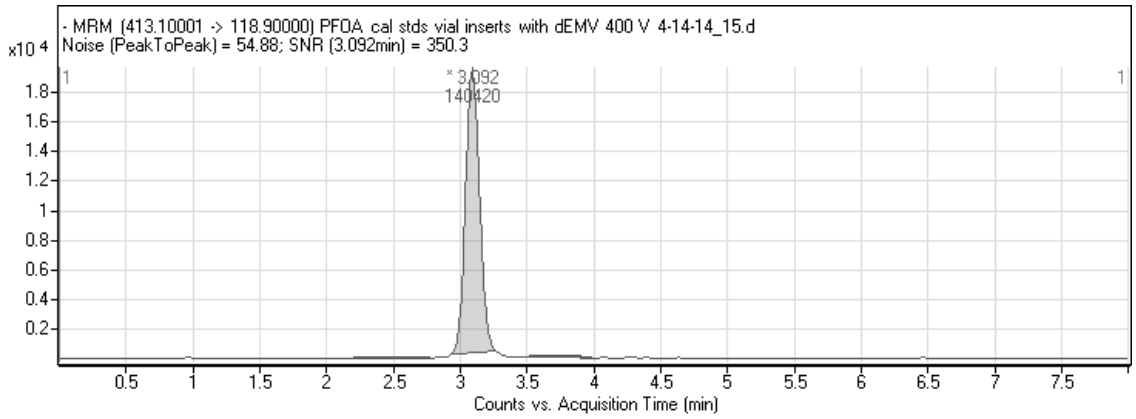

Figure 29. The MRM chromatogram of the 413 → 119 *m/z* transition of 6 μM PFOA obtained from method 3. PFOA has a retention time of 3.092 min, a peak area of 1.40×10^5 counts•min, and a signal-to-noise ratio (SNR) of 350.3.